


The interplay between $\alpha 7$ nicotinic acetylcholine receptors, pannexin-1 channels and P2X7 receptors elicit exocytosis in chromaffin cells

María C. Maldifassi¹ | Fanny Mombousse² | María J. Guerra¹ | Alex H. Vielma¹ | Jaime Maripillán¹ | Ximena Báez-Matus¹ | Carolina Flores-Muñoz^{1,3} | Bárbara Cádiz^{1,4} | Oliver Schmachtenberg¹ | Agustín D. Martínez¹ | Ana M. Cárdenas¹ 

¹Centro Interdisciplinario de Neurociencia de Valparaíso, Facultad de Ciencias, Universidad de Valparaíso, Valparaíso, Chile

²Institut Pasteur, Paris, France

³Programa de Doctorado en Ciencias, Universidad de Valparaíso, Chile

⁴Programa de Magister en Ciencias Biológicas, Universidad de Valparaíso, Chile

Correspondence

Ana M. Cárdenas, Gran Bretaña 1111, Valparaíso, Chile.
Email: ana.cardenas@uv.cl

Agustín D. Martínez, Gran Bretaña 1111, Valparaíso, Chile.
Email: agustin.martinez@uv.cl

Funding information

FONDECYT, Grant/Award Number: 3180140, 1161672 and 1171240; ICM-ANID, Grant/Award Number: P09-022-F; Ministerio de Ciencia

Abstract

Pannexin-1 (Pax1) forms plasma membrane channels that allow the exchange of small molecules between the intracellular and extracellular compartments, and are involved in diverse physiological and pathological responses in the nervous system. However, the signaling mechanisms that induce their opening still remain elusive. Here, we propose a new mechanism for Pax1 channel activation through a functional crosstalk with the highly Ca^{2+} permeable $\alpha 7$ nicotinic acetylcholine receptor (nAChR). Consistent with this hypothesis, we found that activation of $\alpha 7$ nAChRs induces Pax1-mediated dye uptake and ATP release in the neuroblastoma cell line SH-SY5Y- $\alpha 7$. Using membrane permeant Ca^{2+} chelators, total internal reflection fluorescence microscopy in SH-SY5Y- $\alpha 7$ cells expressing a membrane-tethered GCAMP3, and Src kinase inhibitors, we further demonstrated that Pax1 channel opening depends on Ca^{2+} signals localized in submembrane areas, as well as on Src kinases. In turn, Pax1 channels amplify cytosolic Ca^{2+} signals induced by the activation of $\alpha 7$ nAChRs, by a mechanism that seems to involve ATP release and P2X7 receptor activation, as hydrolysis of extracellular ATP with apyrase or blockage of P2X7 receptors with oxidized ATP significantly reduces the $\alpha 7$ nAChR- Ca^{2+} signal. The physiological relevance of this crosstalk was also demonstrated in neuroendocrine chromaffin cells, wherein Pax1 channels and P2X7 receptors contribute to the exocytotic release of catecholamines triggered by $\alpha 7$ nAChRs, as measured by amperometry. Together these findings point to a functional coupling between $\alpha 7$ nAChRs, Pax1 channels and P2X7 receptors with physiological relevance in neurosecretion.

KEYWORDS

Ca^{2+} signals, chromaffin cells, exocytosis, P2X7 receptor, Pannexin-1, $\alpha 7$ nAChRs

Abbreviations: ¹⁰Pannexin-1, 10Pax; ACh, acetylcholine; AChR, acetylcholine receptor; AU, arbitrary units; BGTX, α -bungarotoxin; BSA, bovine serum albumin; Cbx, carbenoxolone; DAPI, 4,6-diamidino-2-phenylindole; Dh β E, dihydro- β -erythroidine hydrobromide; DMEM/F-12, Dulbecco's Modified Eagle's medium/nutrient mixture F-12; DMPP, dimethylphenylpiperazinium; DMSO, dimethyl sulfoxide; FBS, fetal bovine serum; HBSS, Hanks' balanced salt solution; MLA, methyllycaconitine; nAChR, nicotinic acetylcholine receptor; NT, non-treated; oATP, oxidized ATP; P2X7R, P2X7 receptor; Pax1, pannexin-1; PBN, probenecid; PFA, p-formaldehyde; PMSF, phenylmethyl sulfonylfluoride; PVDF, polyvinylidene fluoride membranes; RRID, Research Resource Identifier; Scrbld, scrambled; TIRF, total internal reflection fluorescence.



1 | INTRODUCTION

Pannexins comprise a three membered family of plasma membrane glycoproteins that assemble as heptameric or octameric channel structures (Ambrosi et al., 2010; Jin et al., 2020; Michalski et al., 2020; Mou et al., 2020). When activated, these channels allow the exchange of small molecules, including ATP, between the intracellular and extracellular compartments (Bao et al., 2004; Dahl, 2015; Huang et al., 2007; Locovei et al., 2006; Penuela et al., 2013). The highly ubiquitous pannexin isoform pannexin-1 (Panx1) is involved in diverse physiological/pathological conditions in the nervous system, including neuroplasticity and neuropathic pain (Ardiles et al., 2014; Bravo et al., 2014; Spray & Hanani, 2017; Yeung et al., 2020).

Panx1 channels open at positive membrane potentials (Bruzzone et al., 2003), and also seem to be activated by high extracellular K^+ concentrations (Silverman et al., 2009), elevated cytosolic Ca^{2+} (Locovei et al., 2006), tyrosine phosphorylation by Src kinase (Iglesias et al., 2008; Lohman et al., 2015; Weillinger et al., 2012), and caspase cleavage of its C-terminal autoinhibitory domain (Boyd-Tressler et al., 2014; Chiu et al., 2017; Sandilos et al., 2012). However, further investigation is required to demonstrate the relevance of these mechanisms (Chiu et al., 2018). Different studies have also shown that Panx1 channels are functionally coupled to the P2X7 purinergic receptor (P2X7R). In this cross-talk, activation of P2X7Rs leads to Panx1 channel opening with the subsequent release of ATP, a signaling molecule recognized by P2X7Rs (Sáez et al., 2017; Tozzi et al., 2018), or by other purinergic receptors, including P2Y₁ (Pinheiro, et al., 2013), P2Y₂ (Zhang et al., 2012), P2Y₆ (Silva et al., 2015; Timóteo et al., 2014) and P2Y₁₂ receptors (Pinheiro, et al., 2013). The P2X7R is an ATP-gated ion channel permeable to Na^+ , K^+ , and Ca^{2+} that can also form a macropore permeable to large molecules (<900 Da) during prolonged stimulation (Di Virgilio et al., 2018). Some evidence pointed Panx1 as part of the molecular entity that constitutes the ATP-activated macropore (Locovei et al., 2007), but other findings support that the macropore is an intrinsic property of the P2X7R channel (Di Virgilio et al., 2018). The mechanism that leads to this macropore formation remains elusive (Ugur & Ugur, 2019).

We previously demonstrated that Panx1 channels enhance Ca^{2+} transients and exocytosis driven by the activation of nicotinic acetylcholine receptors (nAChRs; nomenclature follows Zoli et al., 2018) in bovine chromaffin cells (Momboisse et al., 2014), but the specific nicotinic receptor linked to Panx1 remained to be identified. nAChRs are ligand-gated cation channels made of hetero- or homomeric subunits arranged symmetrically around a central ion pore (Taly et al., 2009). nAChR subunits are encoded by 17 different genes (Taly et al., 2009), and the subunit composition determines the function and pharmacological properties of the receptors (Bouzat & Sine, 2018). Bovine chromaffin cells express homomeric $\alpha 7$ and heteromeric receptors made up of $\alpha 3$ (and possibly $\alpha 5$) and $\beta 4$ subunits (Criado, 2018). Since homomeric $\alpha 7$ nAChRs exhibit high Ca^{2+} permeability, when compared with other nAChRs (Bertrand et al., 2015; Séguéla et al., 1993), and cytosolic Ca^{2+} signals seem to activate

Panx1 channels (Alvarez et al., 2016; Garré et al., 2016; Locovei et al., 2006; Murali et al., 2014), we hypothesized that $\alpha 7$ nAChRs promote Panx1 channel opening, and in turn, Panx1 channels enhance $\alpha 7$ nAChR-elicited cytosolic Ca^{2+} signals. We first tested this hypothesis in SH-SY5Y neuroblastoma cells stably transfected with the $\alpha 7$ nAChR subunit (SH-SY5Y- $\alpha 7$) and then in primary cultured bovine chromaffin cells. By combining dye uptake assays, electrophysiology experiments, total internal reflection fluorescence (TIRF) microscopy in cells expressing a membrane-tethered form of GCAMP3, and amperometry for catecholamine exocytosis measurements, we show that activation of $\alpha 7$ nAChRs leads to Panx1 channel opening by a mechanism that depends on submembrane Ca^{2+} signals and Src kinases. In turn, Panx1 channels amplify cytosolic Ca^{2+} transients and exocytosis events by a mechanism that seems to involve P2X7Rs.

2 | MATERIALS AND METHODS

2.1 | SH-SY5H- $\alpha 7$ cell culture

The SH-SY5Y cell line stably expressing human $\alpha 7$ nAChRs was a generous gift from Dr. D. Feuerbach (Research Foundation, Novartis, Geneva, Switzerland) (Charpantier et al., 2005). Cells were seeded onto 12-mm poly-L-lysine-coated glass coverslips and maintained in Dulbecco's Modified Eagle's medium/nutrient mixture F-12 medium supplemented with 10% fetal bovine serum in a humidified atmosphere containing 5% CO_2 at 37°C. To maintain constitutive selection of transfected cells, the culture medium was supplemented with 100 $\mu g/ml$ of antibiotic G418 (Sigma-Aldrich). The maximum number of passages for this cell line was fifteen. The non-transfected SH-SY5Y cell line is not listed as a commonly misidentified cell line by the International Cell Line Authentication Committee. We did not perform any authentications of this cell line.

2.2 | Bovine adrenal chromaffin cell culture

Chromaffin cells from bovine origin were isolated from adrenal glands acquired from the slaughterhouse "Frigorífico Don Pedro", as previously described (Guerra et al., 2019). In brief, adrenal glands were digested in a solution containing 0.25% collagenase B, 0.01% trypsin inhibitor and 0.5% bovine serum albumin. Afterward, chromaffin cells were isolated by means of Percoll gradient centrifugation, resuspended in a 1:1 mixture of Dulbecco's Modified Eagle's medium/nutrient mixture F-12 medium supplemented with 10% fetal bovine serum and maintained at 37°C in a 5% CO_2 atmosphere.

2.3 | TUNEL assay

Dead cells were detected using the terminal deoxynucleotidyl transferase dUTP nick end labeling (TUNEL) kit (Roche

Diagnostics). SH-SY5Y- α 7 cells incubated with different treatments were fixed in 4% PFA for 20 min, washed with phosphate-buffered saline (PBS, NaCl 137 mM, KCl 2.7 mM, Na₂HPO₄ 10 mM, KH₂PO₄ 1.8 mM, pH 7.4) and permeabilized for 30 min with 0.3% Triton X-100, 0.1% sodium citrate in PBS. The TUNEL reaction was then performed for 1 hr at 37°C. The samples were rinsed in PBS, counter-stained with 4,6-diamidino-2-phenylindole (DAPI) and mounted in Dako fluorescent mounting medium (Dako). Images were obtained with a Zeiss AxioImager Z1 microscope (Zeiss AxioImager Z1 with Apotome 1 attachment, objective 63x, NA 1.4) (Table 1).

2.4 | Immunoblot assay for Panx1

Panx1 protein expression was determined in SH-SY5Y- α 7 cells, primary mouse microglia and GH3 cells. Briefly, cells were lysed in a non-denaturing lysis buffer (300 mM NaCl, 5 mM EDTA, 50 mM TRIS HCl, 1% Triton X-100, 1 μ M phenylmethyl sulfonylflouride, 0.1 mM leupeptine, 50 mM NaF, 0.2 mM Na₃VO₄). Protein content was quantified using the Quant-it Protein Assay Kit (Invitrogen). A total of 40 μ g of proteins were separated by SDS-PAGE on a 10% polyacrylamide gel and were transferred electrophoretically to polyvinylidene fluoride membranes. Afterward, membranes were incubated with PBS containing 5% bovine serum albumin and 1% Tween-20 for 2 hr, and then incubated overnight at 4°C with polyclonal antibodies against Panx1 (1:1.000) or β -tubulin (1:1.000) for loading control. After primary antibody incubation and washing, membranes were incubated with a secondary donkey anti-rabbit horseradish peroxidase (HRP) antibody (1:5.000) or with an anti-sheep HRP antibody (1:5.000) for 1 hr. Immunoreactive detection was carried out using the ECL Plus system (Amersham GE Lifes Sciences), and specific bands were detected using the image acquisition system Epichem³ Darkroom. The ImageJ 1.43 analysis software was used for quantification (NIH). Information on the antibodies used in this study is shown in Table 2.

2.5 | Immunofluorescence

Cultured SH-SY5Y- α 7 cells or bovine chromaffin cells were rinsed with PBS and fixed with 4% PFA for 15 min. Afterward, cells were permeabilized with a solution containing 0.2% Triton X-100 for 30 min and labeled overnight with the anti-Panx1 antibody (1:100) or anti-P2X7 antibody (1:100) in PBS containing 5% normal goat serum at room temperature, followed by incubation with AlexaFluor 488 goat anti-rabbit IgG (1:1.000) or AlexaFluor 555 goat anti-rabbit IgG (1:1.000) for 2 hr at room temperature. Subsequently, cell nuclei were stained with DAPI for 15 min, rinsed with PBS and mounted with Dako fluorescent mounting medium (Dako). Cells were visualized with a Nikon C1 Plus laser-scanning confocal microscope

TABLE 1 List of chemicals used in this study

Name	Catalog No.	Source
BGTX	2133	Tocris
BAPTA-AM	A1076	Merk Company
BSA	A7906	Sigma-Aldrich
Cbx	C4790	Sigma-Aldrich
Collagenase B	11088807001	Roche
Dako mounting medium	S3023	Dako
DAPI	D9542	Sigma-Aldrich
DH β E	2349	Tocris
DMPP	D5891	Sigma-Aldrich
DMSO	276855	Sigma-Aldrich
DMEM/F-12	12400-024	Gibco
EGTA-AM	99590-86-0	Calbiochem
FBS	16000-044	Gibco
Fluo-4 a.m.	F14201	Invitrogen
Fura-2 a.m.	F1221	Invitrogen
Gentamicin	15750078	Gibco
Goat serum	G9023	Sigma-Aldrich
HBSS	14025134	Gibco
Leupeptine	78435	Thermo-Fisher
MLA	1029	Tocris
NaF	106449	Merck
Na ₃ VO ₄	S6508	Sigma-Aldrich
Percoll	17089101	GE Healthcare
¹⁰ Panx	3348	Tocris
Scrbld	3708	Tocris
PFA	158127	Sigma-Aldrich
PMSF	P7626	Sigma-Aldrich
PNU-1205696	P0043	Sigma-Aldrich
Poly-L-lysine	P4707	Sigma-Aldrich
PP2	1407	Tocris
PP3	2794	Tocris
PBN	P8761	Sigma-Aldrich
Triton X-100	9036-19-5	Merk Company
oATP	A6779	Sigma-Aldrich
Apyr	A6535	Sigma-Aldrich

Abbreviations: ¹⁰Panx, ¹⁰Pannexin-1; BGTX, α -bungarotoxin; BSA, bovine serum albumin; Cbx, carbenoxolone; DAPI, 4,6-diamidino-2-phenylindole; Dh β E, dihydro- β -erythroidine hydrobromide; DMEM/F-12, Dulbecco's Modified Eagle's medium/nutrient mixture F-12; DMPP, dimethylphenylpiperazinium; DMSO, dimethyl sulfoxide; FBS, fetal bovine serum; HBSS, Hanks' balanced salt solution; MLA, methyllycaconitine; nAChR, nicotinic acetylcholine receptor; NT, non-treated; oATP, oxidized ATP; P2X7R, P2X7 receptor; Panx1, pannexin-1; PBN, probenecid; PFA, p-formaldehyde; PMSF, phenylmethyl sulfonylflouride; PVDF, polyvinylidene fluoride membranes; RRID, Research Resource Identifier; Scrbld, scrambled.



Name	Catalog No.	RRID	Source
Anti- β -tubulin	ATN02	AB_10709401	Cytoskeleton
Anti-Panx1	ab139715	AB_10900459	Abcam
Peroxidase affiniPure F(ab') ₂ fragment donkey anti-rabbit IgG	711-036-152	AB_2340590	Jackson ImmunoResearch
HRP-conjugated donkey anti-sheep IgG	A16041	AB_2534715	Thermo Fisher Scientific
Alexa Fluor 488 goat anti-rabbit IgG	A11008	AB_143165	Thermo Fisher Scientific
Anti-P2X7	ab77413	AB_2158249	Abcam
Alexa Fluor 555 goat anti-rabbit IgG	A32732	AB_2633281	Thermo Fisher Scientific

TABLE 2 List of antibodies used in this study, including Research Resource Identifier (RRID)

(Nikon), equipped with a 60 \times objective (NA 1.49). The information on the antibodies used in this study is described in Table 2.

2.6 | Time-lapse imaging of DAPI uptake

Cultured SH-SY5Y- α 7 cells were seeded onto 25-mm poly-L-lysine-coated glass coverslips, and 24 hr later DAPI uptake was evaluated. The cells were rinsed twice with Hanks' balanced salt solution containing 2 mM Ca²⁺, and incubated in Hanks' balanced salt solution plus 50 μ M DAPI. After 500 s, cells were stimulated with 1 mM acetylcholine (ACh), and after 1,500 s the vehicle or probenecid (PBN) was added to a final concentration of 200 μ M. Fluorescence images were obtained using a 40 \times objective in an inverted microscope (Eclipse Ti-E; Nikon). Images were acquired with a cooled digital camera (ORCA-FLASH 2.0; Hamamatsu Photonics) and NIS-Element Advanced Research 4.3 software (Nikon). Time-lapse images were acquired at 200 ms intervals in stream mode at room temperature. Data are shown as F/F_0 ratio, where F_0 and F are the background-subtracted fluorescence intensities recorded immediately before and after the addition of ACh, respectively. Changes in the F/F_0 slope were compared with regression lines fitted to data points using Microsoft Excel. No protocol for studying nAChR desensitization has been used in these experiments.

2.7 | DAPI uptake snapshot

DAPI uptake was measured using a snapshot protocol previously described by Mombouisse et al. (2014). Briefly, SH-SY5Y- α 7 stable cells or bovine chromaffin cells were washed twice with Krebs-HEPES solution (in mM: 140 NaCl, 5.9 KCl, 1.2 MgCl₂, 2 CaCl₂, 10 HEPES-NaOH, 10 glucose, pH 7.4) and incubated for 15 min in Krebs-HEPES solution with or without the corresponding inhibitors at 37°C. Afterward, cells were incubated for 10 s in a Krebs-HEPES solution with 50 μ M DAPI in the absence or presence of 50 μ M dimethylphenylpiperazinium (DMPP), 100 μ M acetylcholine or 10 mM choline and the respective inhibitors. Next, cells were washed with Krebs-HEPES solution for 2 min, fixed in 4% PFA for 15 min, and mounted

with DAKO fluorescent mounting medium. Cells were visualized with a Nikon C1 Plus laser-scanning confocal microscope (Nikon), and excited with a 408 nm laser line. All images were captured at the equatorial plane of the cells using identical exposure settings between compared samples. Confocal acquisitions were analyzed and processed using NIS-Elements Viewer 4.0 software (Nikon). DAPI uptake was determined by calculating the fluorescence intensity of each cell nucleus corrected by background fluorescence and divided by nucleus area, and expressed as arbitrary units (AU) per cell nucleus area (AU/ μ m²). For each coverslip, 10–60 cells were analyzed, and DAPI fluorescences were averaged. Uptake data were normalized to non-treated (NT) condition per day of experiment.

2.8 | ATP release

A luciferin/luciferase-based ATP Determination Kit (Molecular Probes, Invitrogen) was used to quantify ATP release. In brief, stably transfected SH-SY5Y- α 7 cells were seeded in a 24-well plaque. After 24 hr, culture medium was replaced with fresh culture medium or medium containing the corresponding inhibitors for 15 min at 37°C. Thereafter, the medium was replaced with medium containing 50 μ M DMPP with or without the appropriate inhibitors for 10 min at 37°C. Culture supernatant was stored at –80°C until used. For ATP quantification, 10 μ l of each sample was mixed with 90 μ l of ATP-reaction solution following the manufacturer's instructions. ATP concentration was determined using an ATP calibration curve ranging from 1 nM to 1 μ M, and measured with an Appliskan Luminometer (Thermo Electro Corporation) together with the SkanIT software (Thermo Electro Corporation). As control, standard curves were made with ATP at a concentration ranging from 1 nM to 1 μ M in the presence of each inhibitor at the respective concentration. No effect of inhibitors over the sensitivity of ATP detection was observed.

2.9 | Cytosolic Ca²⁺ measurements

SH-SY5Y- α 7 cells were incubated with the Ca²⁺ sensitive indicator Fluo-4a.m. (5 μ M), for a period of 30 min at 37°C. Afterward,

the cells were incubated in recording solution with or without the corresponding inhibitors together or not with PNU-1205696 for 10 min prior to and during stimulation with DMPP. Ca^{2+} transients were assessed using a 40 \times objective on an inverted microscope (Eclipse Ti-E; Nikon). Images were acquired with a cooled digital camera (ORCA-FLASH 2.0; Hamamatsu Photonics) and NIS-Element Advanced Research 4.3 software (Nikon). Data are shown as F/F_0 ratio, where F_0 and F are the background-subtracted fluorescence intensities recorded immediately before and after the addition of DMPP, respectively. At least 10 cells per coverslip were analyzed and cell fluorescences were averaged.

Ca^{2+} transients in bovine chromaffin cells were measured using the Ca^{2+} -sensitive indicator Fura-2 a.m. Cells were seeded onto 25-mm poly-L-lysine-coated glass coverslips. Forty-eight later, the cells were incubated with 5 μM Fura-2 a.m. for 30 min at room temperature. Afterward, the cells were incubated in recording solution with or without the corresponding inhibitors together or not with PNU-1205696 for 10 min prior to and during stimulation with choline. Each coverslip was mounted on a Nikon Eclipse Ti-inverted microscope, and imaged with NIS-Elements software (Nikon). Fluorescence intensity was captured every 1 s at 340 and 380 nm excitation wavelengths and emission at 510 nm. Individual fluorescent ratiometric signals ($F = 340/380$ nm excitation ratio) were automatically calculated by the software. The basal fluorescence (F_0) was calculated before addition of nAChR ligands, and to plot fluorescence variations over time, fluorescent signals at each time point were normalized to the basal level F_0 (F/F_0 ratio).

2.10 | Measurements of submembrane Ca^{2+} signals

For the detection of local Ca^{2+} transients in the submembrane area, SH-SY5Y- $\alpha 7$ cells were transfected with the genetically encoded Ca^{2+} indicator GCaMP3 modified to include a membrane-tethering domain, pN1-Lck-GCaMP3, a gift from Baljit Khakh (Addgene plasmid # 26974) (Shigetomi et al., 2010). Cells were transfected with 1 μg of DNA using Lipofectamine 2000 according to the manufacturer's instructions. Twenty-four hours post transfection, cells were imaged using an inverted microscope (Eclipse Ti-E; Nikon) with a 100 \times APO TIRF objective (NA 1.49; Nikon) and a Perfect Focus Unit (TI-ND6-PFS; Nikon). Lck-GCaMP3 transfected cells were illuminated with a 488 nm laser (488-20LS, OBIS; Coherent). TIRF images were acquired at 100 ms intervals in stream mode. To determine relative changes in the fluorescence signals, three regions of interest (ROIs) were selected for each cell, and the background obtained from a neighboring area was subtracted from each ROI. The three normalized ROIs were averaged to yield the mean values. Data are represented as F/F_0 values, where F_0 is the fluorescence at resting condition.

2.11 | Amperometric recordings

Amperometric recordings were done as formerly described (González-Jamett et al., 2017). In brief, 5 μm diameter carbon fibers

(Thornel P-55; Amoco Performance Product) were held at a potential of 650 mV in order to detect single exocytotic events. A HEKA EPC10 amplifier (HEKA Elektronik; Lambrecht/Pfalz) controlled by PatchMaster software (HEKA Elektronik) was used to obtain the amperometric signals, which were low pass filtered at 1 kHz and digitized at 5 kHz. Cells were maintained in Krebs-HEPES solution throughout the recordings. Exocytosis was elicited by a 10 s pressure ejection of 50 μM DMPP using a custom-made picospritzer operating at a pressure of 2–3 psi. In some experiments, cells were pre-incubated for 15 min with the corresponding blockers or inhibitors and were maintained in the bath solution during the entire recording. Exocytotic events were analyzed using a custom-written macro for IGOR PRO (Wavemetrics), obtained from Dr. R. Borges. The analysis was restricted to spikes with amplitudes ≥ 10 pA, foot amplitudes ≥ 3 pA and foot durations ≥ 3 ms. Each amperometric parameter was statistically analyzed by taking the median values from individual cells and then averaging these values per treatment group.

2.12 | Patch clamp electrophysiology in chromaffin cells

Patch clamp recordings were made from bovine chromaffin cells at 48 hr post-seeding. Cells were visualized with an Olympus microscope (BX51WI; Olympus) equipped with a 40 \times water immersion objective, infrared differential interference contrast and a cooled CCD camera (DS-2MBWc; Nikon) for bright-field image capture. Cells were voltage clamped at -60 mV in whole-cell configuration. Signals were amplified with an EPC7-plus amplifier (HEKA Elektronik; Lambrecht), filtered at 3 kHz, digitized and sampled at 10 kHz with an A/D board (PCI-6221; National Instruments) and recorded using custom-made software written in IGOR PRO (Wavemetrics). Electrodes were fabricated using borosilicate glass capillaries (1.5 mm OD, 0.84 mm ID; WPI) and pulled to resistances between 10 and 15 MV on a Flaming/Brown electrode puller (Sutter P-97; Sutter Instruments). Recording electrodes were filled with an internal solution composed of (in mM): 125 potassium gluconate, 10 KCl, 10 HEPES, 2 EGTA, 2 Na₂ATP, 2 NaGTP, pH 7.4. In some experiments, cells were pre-incubated for 15 min with the corresponding blockers or inhibitors and were maintained in the bath solution during the whole recording. Cells were voltage-clamped, and were stimulated with 1 s pressure ejection of 50 μM DMPP using a custom-made picospritzer operating at 2–3 psi of pressure. The maximum amplitude of the DMPP response was measured at the peak of the fast component compared to baseline, using IGOR PRO. Decay rate of the DMPP response was also measured using IGOR PRO software.

2.13 | Study design and statistics analysis

This study was not pre-registered. No randomization was performed. Outliers were identified using the Grubbs Method, also known as

ESD (extreme studentized derivative; GraphPad Software Inc, La Jolla, CA, USA; web page for free access: <https://www.graphpad.com/quickcalcs/Grubbs1.cfm>). Researchers were not blinded during the experiments. Sample sizes were not statistically pre-determined, but estimated based on previous studies (del Barrio et al., 2011; Guerra et al., 2019; Harcha et al., 2019). Results are expressed as means \pm SEM. According to the Kolmogorov–Smirnov test, not all data were normally distributed. Normally distributed data were analyzed using one-way ANOVA followed by Bonferroni's post hoc test, and non-normally distributed data with the Kruskal–Wallis test followed by Dunn's post hoc test. All statistical analyses were performed using GraphPad Prism software version 5.0 (GraphPad Software Inc.).

2.14 | Ethics statement

This research was approved by the Biosafety and Bioethics committees of Universidad de Valparaíso (Chile), approval identification numbers BS002-18 and BEA119-18, respectively. Furthermore, the investigators followed the Manual of Biosafety Regulations stipulated by CONICYT (Chile) version 2008, CDC (USA) Biosafety Manual 4th Edition, and Laboratory Biosafety, WHO, Geneva, 2005; mainly in reference to experiments with recombinant DNA and RNA and the manipulation of cell lines. This work includes the use of bovine adrenal glands obtained from a local slaughterhouse, Frigorific Don Pedro, certificated (Livestock role 04.2.03.0002 from the Agriculture and Livestock Service of the Chilean Government). The slaughterhouse is regularly inspected by a veterinarian of the Chilean Health Service. Transport, processing, and elimination of the samples were carried out in strict accordance with the Article 86 of the Sanitary Regulations of the Chilean Government (Supreme decree Nu 977/96).

3 | RESULTS

3.1 | Panx1 channels expressed in the SH-SY5Y- α 7 cell line are activated by acetylcholine

To study the crosstalk between α 7 nAChRs and Panx1 channels, we took advantage of SH-SY5Y- α 7 cells that stably over-express α 7 nAChR (Charpantier et al., 2005; Guerra-Álvarez et al., 2015). In agreement with a previous report in the parental SH-SY5Y cell line (Wilkaniec et al., 2017), we further corroborated by immunofluorescence and immunoblot that SH-SY5Y- α 7 cells express Panx1 (Figure 1a,b). Under confocal microscopy, Panx1 labeling is observed in both intracellular and cell surface compartments (Figure 1a). In the immunoblot analysis, Panx1 protein was detected as a band of about 48 kDa (Figure 1b), as in pituitary-derived GH3 and mouse primary microglial cell extracts, which are known to express this protein (Li et al., 2011; Orellana et al., 2011).

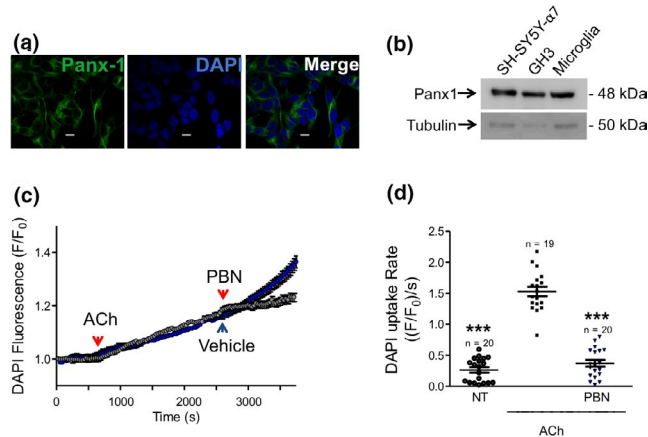


FIGURE 1 Activation of Panx1 channel by acetylcholine (ACh) in SH-SY5Y- α 7 cells. (a) Immunofluorescent detection of Panx1 in SH-SY5Y- α 7 cell line. Panx1 was labeled using an anti-Panx1 antibody, and visualized with an Alexa Fluor 488 secondary antibody. 4,6-diamidino-2-phenylindole (DAPI) was used to stain nuclei. Scale bar 10 μ m. (b) Immunoblot of Panx1 in the SH-SY5Y- α 7, pituitary-derived GH3 and mouse primary microglial cell extracts. (c) Time-lapse detection of DAPI uptake in SH-SY5Y- α 7 cells. Fluorescent images were acquired at 1 Hz. Time of addition of ACh (final concentration: 1 mM), probenecid (PBN; final concentration: 200 μ M) or the vehicle DMSO, is indicated with red arrows. Blue dots correspond to the experiments where only ACh was added ($n = 15$ cells from different experiments ($N = 3$)); gray dots correspond to the experiment where PBN was added after ACh addition ($n = 20$ cells from different experiments ($N = 3$)). Data are shown as F/F_0 ratio, where F is the background-subtracted fluorescence intensity during the recording and F_0 is the background-subtracted fluorescence intensity at the start of the experiment. Each value corresponds to the mean \pm SEM. Note that ACh induced a fast increment in the rate of DAPI uptake that was significantly slowed after addition of the Panx1 blocker PBN (gray). (d) DAPI uptake rate (uptake slope) in the non-treated (NT) condition and after treatment with ACh in the absence or presence of PBN. Dots represent DAPI uptake slopes

TAKEN

from individual cells ($n = 20$) from three different cell cultures ($N = 3$). Horizontal lines and whiskers indicate means and SEM. *** $p < .001$ compared with the ACh condition (one-way ANOVA followed by Bonferroni's post hoc test)

Next, we evaluated whether ACh promotes the opening of Panx1 channels, at a concentration (1 mM) that induces alpha-bungarotoxin (BGTX)-sensitive whole-cell currents in SH-SY5Y- α 7 cells (Charpantier et al., 2005). Panx1 channel activation was measured by time-lapse imaging of DAPI uptake. As shown in Figure 1c,d, upon stimulation with 1 mM ACh, SH-SY5Y- α 7 cells took up the tracer with increasing rate ($1.5 \pm 0.08 F/F_0 s^{-1}$) compared to the NT condition ($0.26 \pm 0.04 F/F_0 s^{-1}$). This uptake rate was reduced in the presence of 200 μ M PBN ($0.37 \pm 0.05 F/F_0 s^{-1}$), a Panx1 channel blocker (Silverman et al., 2008). The vehicle (dimethyl sulfoxide, DMSO) did not reduce the uptake rate (Figure 1c). These findings suggest the expression of functional Panx1 channels activated by cholinergic receptors in SH-SY5Y- α 7 cells.

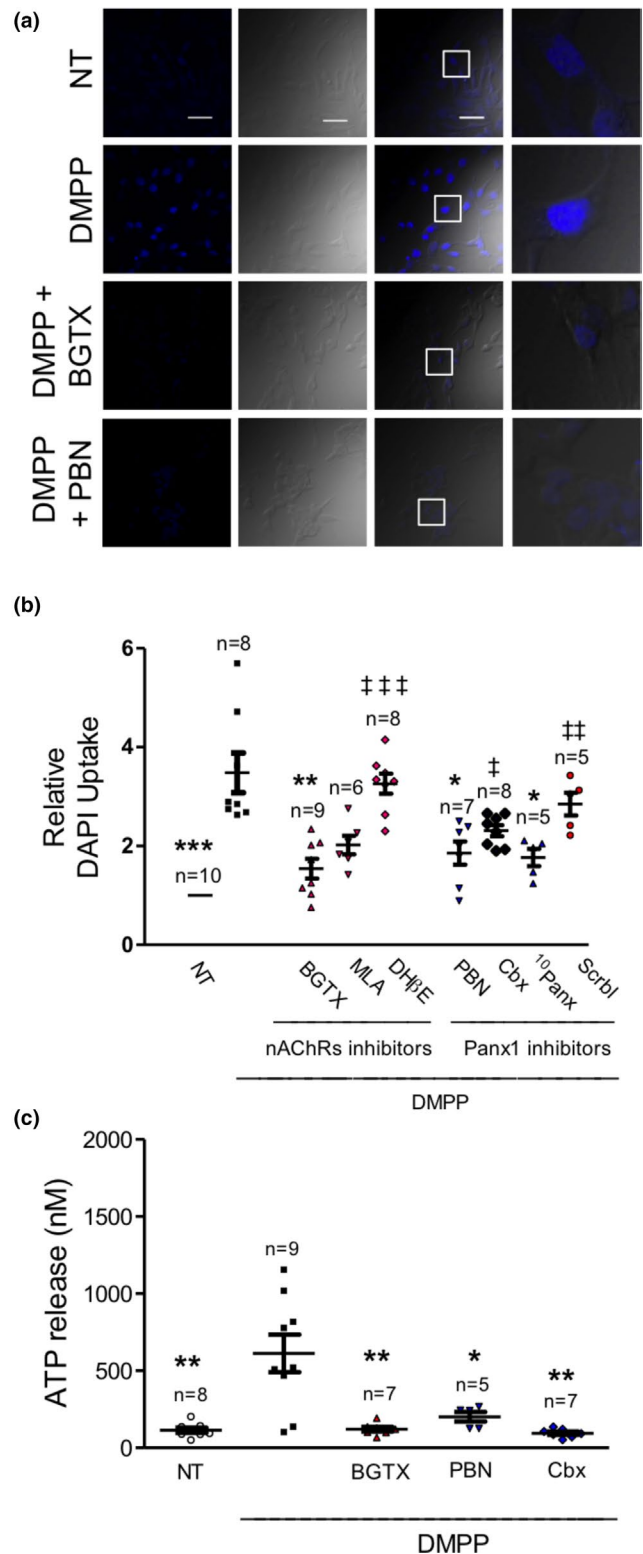
3.2 | $\alpha 7$ nAChRs activate Panx1 channels in the SH-SY5Y- $\alpha 7$ cell line

Next, we assessed the specific contribution of $\alpha 7$ nAChRs to the opening of Panx1 channels using a previously described dye uptake snapshot protocol (Momboisse et al., 2014). DAPI uptake was measured in SH-SY5Y- $\alpha 7$ cells stimulated with 50 μ M of the nAChR agonist DMPP in the presence of selective antagonists of $\alpha 7$ nAChRs and Panx1 channel blockers. Two selective $\alpha 7$ nAChRs antagonists, BGTX and methyllycaconitine (MLA), and three different inhibitors of Panx1 channels, PBN, carbenoxolone (Cbx) and the peptide 10 Panx1, were used. An inactive scrambled peptide analog was used as a control of 10 Panx1. Figure 2a shows examples of images of DAPI uptake in SH-SY5Y- $\alpha 7$ cells NT or stimulated with DMPP in the absence or presence of the $\alpha 7$ nAChR inhibitor BGTX or the Panx1 channel blocker PBN. As shown in Figure 2b, 50 μ M DMPP increased relative uptake (3.5 ± 0.4 times over NT uptake values; $p < .001$). This increased uptake was significantly reduced by 100 nM BGTX (1.5 ± 0.2 times over NT uptake), but less affected by 10 nM MLA (2.0 ± 0.2 times over the NT condition; non-significantly different from both NT and DMPP conditions). SH-SY5Y cells express $\alpha 3$ receptors (Lukas et al., 1993), which can form heteromeric $\alpha 7\alpha 3$ receptors and have less sensitivity toward than to BGTX (Tsuneki et al., 2003). This might explain the lower effect of MLA.

We also evaluated the effect of DH β E, a selective antagonist of $\beta 2^*$ nAChR, a receptor present in SH-SY5Y cells (del Barrio et al., 2011). As shown in Figures 2b 1 μ M DH β E did not affect DMPP-induced dye uptake (3.3 ± 0.2 times over NT uptake). The Panx1 channel blockers

PBN and 10 Panx1, at concentrations that selectively inhibit Panx1 channels (Bruzzone et al., 2005; Silverman et al., 2008) also significantly decreased DAPI uptake (1.9 ± 0.2 and 1.8 ± 0.2 times over NT uptake, respectively). On the other hand, the Panx1 channel blocker Cbx reduced dye uptake without statistical significance (2.3 ± 0.1 times over NT uptake). The scrambled peptide did not significantly affect the DMPP-induced dye uptake (2.8 ± 0.2 times over NT

FIGURE 2 Activation of $\alpha 7$ nicotinic acetylcholine receptors (nAChRs) promotes 4,6-diamidino-2-phenylindole (DAPI) uptake and ATP release in SH-SY5Y- $\alpha 7$ cells. (a, b) DAPI uptake was induced with 50 μ M dimethylphenylpiperazinium (DMPP) without or with pre-treatments with the $\alpha 7$ nAChR antagonists α -bungarotoxin (BGTX; 100 nM) or methyllycaconitine (MLA; 10 nM), the $\alpha 4\beta 2$ nAChR antagonist Dihydro- β -erythroidine (DH β E; 1 μ M), the Panx1 channel blockers probenecid (PBN) (200 μ M), carbenoxolone (Cbx; 5 μ M) or 10 Panx1 (200 μ M), or the scrambled peptide (Scrb1; 200 μ M). (a) Representative confocal image of DAPI uptake (snapshot protocol) in cells NT or stimulated with 50 μ M DMPP for 10 s with or without pre-treatments with BGTX or PBN. Scale bar 10 μ m. (b) DAPI uptake is represented as relative uptake compared to the NT condition. Dots represent average values from individual coverslips. Horizontal lines and whiskers indicate means and SEM, respectively. The number of coverslips analyzed from different cell cultures ($N \geq 3$) is indicated above each bar; 13–56 cells were analyzed for each coverslip. * $p < .05$, ** $p < .01$, *** $p < .001$ compared to DMPP condition; † $p < .05$, †† $p < .01$, ††† $p < .001$ compared to NT condition (Kruskal–Wallis test followed by Dunn's post hoc test). (c) ATP release from SH-SY5Y- $\alpha 7$ was induced by 50 μ M DMPP with or without pretreatment with the respective inhibitors. Each dot represents ATP release from individual culture wells. Horizontal lines and whiskers indicate means and SEM, respectively. The number of experiments is indicated above each bar. (b, c) * $p < .05$, ** $p < .01$, compared to DMPP condition (one-way ANOVA followed by Bonferroni's post hoc test)





uptake). A TUNEL assay was used to determine whether incubation with the aforementioned compounds affected cell viability, producing a false-positive DAPI uptake. No positive nuclei were identified for any condition (Figure S1). Additionally, as control, cells in resting condition were incubated with the $\alpha 7$ nAChRs antagonists and Panx1 channel blockers, and DAPI uptake was assessed. These compounds did not induce uptake by themselves (Figure S2 and Table S1).

Given that activated Panx1 channels are reportedly ATP permeable (Bao et al., 2004; Locovei et al., 2006), we evaluated whether activation of $\alpha 7$ nAChRs elicits ATP release mediated by Panx1 channels. As shown in Figure 2c, ATP concentration in the extracellular medium was 114 ± 16 nM in NT cells and 612 ± 121 nM in cells stimulated with 50 μ M DMPP. This DMPP-induced ATP release was almost completely inhibited by BGTX, PBN or Cbx (121 ± 15 nM, 201 ± 31 nM and 95 ± 11 nM, respectively). Thus, using two complementary experimental approaches, DAPI uptake and ATP release, our results suggest that Panx1 channels are functionally coupled to $\alpha 7$ nAChRs.

3.3 | Panx1 channels are activated by cytosolic Ca^{2+} rises and in turn contribute to Ca^{2+} signals elicited by $\alpha 7$ nAChRs

Since it has been proposed that Panx1 channels are activated by cytosolic Ca^{2+} rises (Locovei et al., 2006), we explored whether this mechanism contributes to the opening of Panx1 channels. We first analyzed the Ca^{2+} signals induced with 50 μ M DMPP in Fluo-4-loaded SH-SY5Y- $\alpha 7$ cells. Figure 3a-upper panel and Movie S1 show SH-SY5Y- $\alpha 7$ cells, in which application of 50 μ M DMPP induced a modest increase in fluorescence. Figure 3a-bottom panel shows averaged fluorescence traces, which reflect relative Ca^{2+} changes. Thus, application of DMPP produced a barely detectable cytosolic Ca^{2+} signal, wherein the mean fluorescence amplitude increased to 1.1 times over basal fluorescence values. This modest cytosolic Ca^{2+} rise might be confined to the immediate vicinity of influx sites. To explore this idea, we decided to measure Ca^{2+} signals in the submembrane area taking advantage of a membrane-tethered GCaM, Lck-GCaMP3 (Shigetomi et al., 2010) together with TIRF microscopy. Figure 3b-upper panel and Movie S2 show a SH-SY5Y- $\alpha 7$ cell expressing Lck-GCaMP3 in the plasma membrane, wherein DMPP stimulation triggered a significant Ca^{2+} increase (1.9 ± 0.19 over basal fluorescence values). Figure 3b-bottom panel shows the maximum amplitude of the F/F_0 signal obtained from three different ROIs in 29 different cells. Thus, the nAChR agonist DMPP induced transient Ca^{2+} elevations detectable only in the submembrane area.

Subsequently, we analyzed the contribution of the Ca^{2+} signals on DMPP-induced Panx1 channel opening using the DAPI uptake protocol in the absence of extracellular Ca^{2+} or in cells loaded with the membrane permeant Ca^{2+} chelators EGTA-AM and BAPTA-AM (Figure 3c). In this set of experiments, DMPP increased the DAPI uptake 3.8 ± 0.5 times over NT uptake. This DAPI uptake increment was not observed in the absence of extracellular Ca^{2+} or in cells

loaded with 20 μ M BAPTA-AM (0.7 ± 0.1 and 1.2 ± 0.1 times over NT uptake, respectively). In the presence of 20 μ M EGTA-AM, DAPI uptake was 1.8 ± 0.2 times over NT uptake, a value non-significantly different from both NT and DMPP conditions.

Because $\alpha 7$ nAChRs can induce the activation of Src kinases (Dasgupta et al., 2006; Kihara et al., 2001; Li et al., 2019; Shen et al., 2012), we also studied the effects of 10 μ M PP2, a Src inhibitor, and its inactive analog PP3 (Traxler et al., 1997). As shown in Figure 3d, in the presence of PP2, DMPP-induced DAPI uptake was 1.8 ± 0.32 times over NT uptake, a value significantly smaller than that induced by DMPP alone. The inactive analog PP3 slightly reduced DMPP-induced DAPI uptake (2.7 ± 0.2 times over NT uptake). Thus, an outcome of nAChR activation is opening of Panx1 channels, which appear to depend on both discrete submembrane Ca^{2+} rises and Src kinases.

Since Panx1 channels amplify Ca^{2+} responses induced by DMPP in chromaffin cells (Momboisse et al., 2014), we analyzed whether Panx1 channels also influence $\alpha 7$ nAChR-induced cytosolic Ca^{2+} signals in SH-SY5Y- $\alpha 7$ cells. Ca^{2+} signals were evoked by 50 μ M DMPP in the presence of PNU-120596, a positive allosteric modulator of $\alpha 7$ nAChR (Hurst et al., 2005), in a concentration range previously used to detect this receptor subtype (del Barrio et al., 2011; Guerra-Álvarez et al., 2015; Maldifassi et al., 2014; Pérez-Alvarez et al., 2012). In this way, we could: (1) promote a detectable cytosolic Ca^{2+} signal, and (2) induce selective activation of $\alpha 7$ nAChR, as SH-SY5Y cells express different types of nAChRs (Antonini et al., 2006; Lukas et al., 1993; Peng et al., 1997). Figure 3e shows averaged fluorescence traces in Fluo-4 loaded SH-SY5Y- $\alpha 7$ cells stimulated with DMPP plus PNU-120596. In this condition, the mean fluorescence amplitude rose to 3.8 ± 0.5 times over basal fluorescence ($p < .01$ compared to the DMPP condition). As shown in Figure 3f, this fluorescence increase was almost completely abolished by 100 nM BGTX, confirming that the cytosolic Ca^{2+} rise was because of $\alpha 7$ nAChR activation, consistent with previous results in this cell line (Guerra-Álvarez et al., 2015). The Panx1 channel inhibitor $^{10}\text{Panx1}$ (200 μ M) also abolished such Ca^{2+} signals, whereas the scrambled peptide had no effects. Thus, the above results suggest that Panx1 channels amplify the Ca^{2+} signals elicited by active $\alpha 7$ nAChR.

3.4 | Panx1 channels are activated by $\alpha 7$ nAChRs and in turn amplify Ca^{2+} response in bovine chromaffin cells

Because an earlier work from our group proposed that Panx1 channels are functionally associated with nAChRs in bovine chromaffin cells (Momboisse et al., 2014), we decided to analyze the possible interaction of Panx1 channels with $\alpha 7$ nAChRs in this cell type. We first studied whether membrane currents induced by DMPP are influenced by Panx1 channels. To this end, cells were clamped at a negative potential (-60 mV), stimulated for 10 s with 50 μ M DMPP, and currents were recorded in the whole cell configuration.

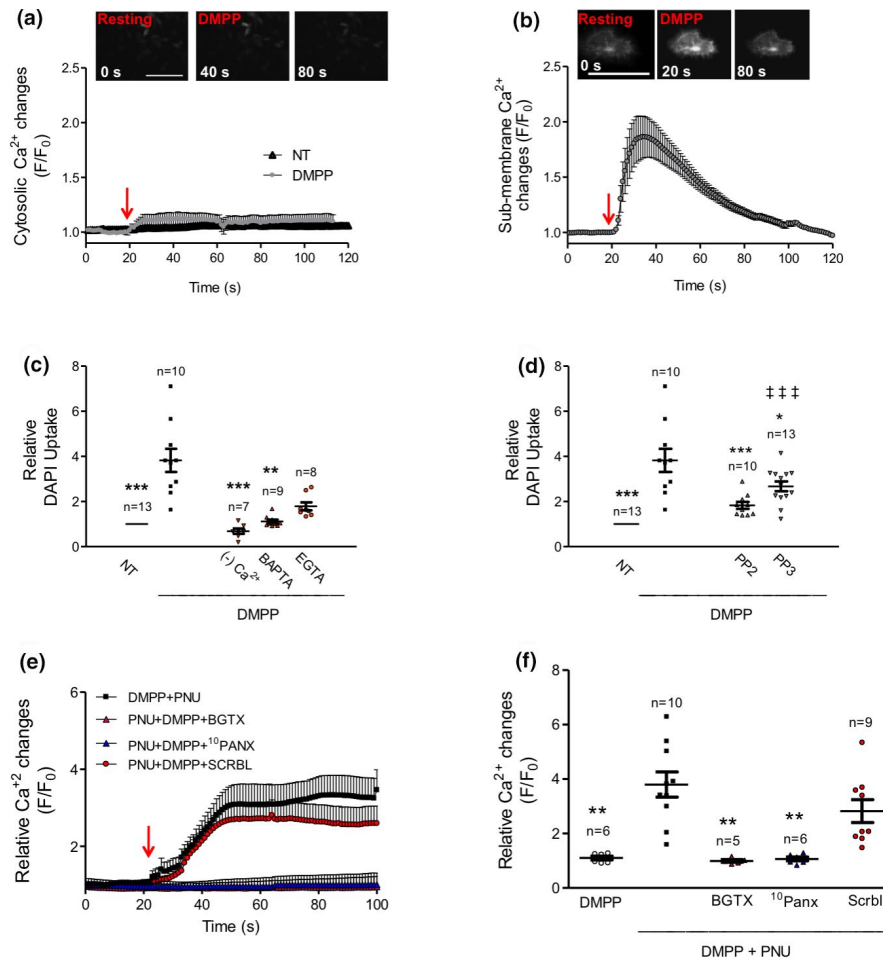


FIGURE 3 $\alpha 7$ nicotinic acetylcholine receptors induce Ca^{2+} -dependent activation of Panx1 channels. (a) Cytosolic Ca^{2+} signals induced with 50 μM dimethylphenylpiperazinium (DMPP) measured in Fluo-4 loaded SH-SY5Y- $\alpha 7$. (b) Submembrane Ca^{2+} signals induced with 50 μM DMPP measured in SH-SY5Y- $\alpha 7$ cells expressing the membrane tethered Ca^{2+} sensor Lck-GCAMP3 using total internal reflection fluorescence microscopy. Top panels show representative images of SH-SY5Y- $\alpha 7$ cells loaded with Fluo-4 (a) or expressing Lck-GCAMP3 (b) before, and during DMPP treatment. Scale bar 10 μm . Bottom graphs show relative changes in fluorescence intensity (F/F_0) in $n = 12$ (a) and $n = 29$ (b) different cells from different cell cultures ($N = 3$). (c) Panx1 channel activation, measured as 4,6-diamidino-2-phenylindole (DAPI) uptake using the snapshot protocol, was induced with 50 μM DMPP under 2 mM extracellular Ca^{2+} , in the absence of extracellular Ca^{2+} ($-\text{Ca}^{2+}$), or in the presence of the permeant Ca^{2+} chelators BAPTA-AM or EGTA-AM at 20 μM . DAPI uptake is represented as relative uptake as compared to the NT condition. $**p < .01$, $***p < .001$ compared to DMPP condition (Kruskal-Wallis test followed by Dunn's post hoc test) (d) DMPP elicited DAPI uptake in the presence of 10 μM of the Src inhibitor PP2 or its inactive analog PP3. DAPI uptake is represented as relative uptake as compared to the NT condition. Dots represent average values from individual coverslips ($n = 13$ –65 cells were analyzed for each coverslip). Horizontal lines and whiskers indicate means and SEM, respectively. The number of coverslips analyzed from independent cultures ($N \geq 3$) is indicated above each bar. $*p < .05$, $***p < .001$ compared to DMPP condition; $†††p < .001$ compared to NT condition (one-way ANOVA followed by Bonferroni's post hoc test). (e, f) Global cytosolic Ca^{2+} signals were measured in Fluo-4 loaded SH-SY5Y- $\alpha 7$ cells stimulated with 50 μM DMPP with or without pre-treatment with 10 μM PNU-1205696 (PNU) in the presence or absence of 100 nM B GTX or 200 μM of the Panx1 channel blocker $^{10}\text{Panx1}$ or the scrambled peptide (Scrbl). (e) Cytosolic Ca^{2+} transients are shown as relative changes in fluorescence intensity (F/F_0). Data represent mean \pm SEM. (f) Each dot represents averaged F/F_0 maximum values from individual coverslips. At least 10 cells per coverslip were analyzed and averaged. Horizontal lines and whiskers indicate means and SEM, respectively. The number of coverslips analyzed from independent cultures ($N \geq 3$) is indicated above each bar. $**p < .01$ compared to DMPP plus PNU condition (one-way ANOVA followed by Bonferroni's post hoc test)

Figure 4a shows representative current traces elicited by local application of DMPP in the absence or presence of 200 μM of $^{10}\text{Panx1}$ or the scrambled peptide. The peak amplitudes of the inward currents elicited under those different conditions were not significantly different (Figure 4b). However, the kinetic properties of DMPP-induced current were significantly faster with the application of 200 μM $^{10}\text{Panx1}$, and not affected by the scrambled peptide (Figure 4c).

Decay values of the currents induced by DMPP were 0.04 ± 0.01 pA/ms in the absence of peptides, 0.15 ± 0.02 pA/ms in the presence of $^{10}\text{Panx1}$, and 0.04 ± 0.01 pA/ms in the presence of the scrambled peptide. These data suggest that Panx1 channels contribute with a slow component to DMPP-induced inward currents.

To confirm the opening of Panx1 channels by activation of $\alpha 7$ nAChRs in chromaffin cells, we evaluated the effects of the $\alpha 7$

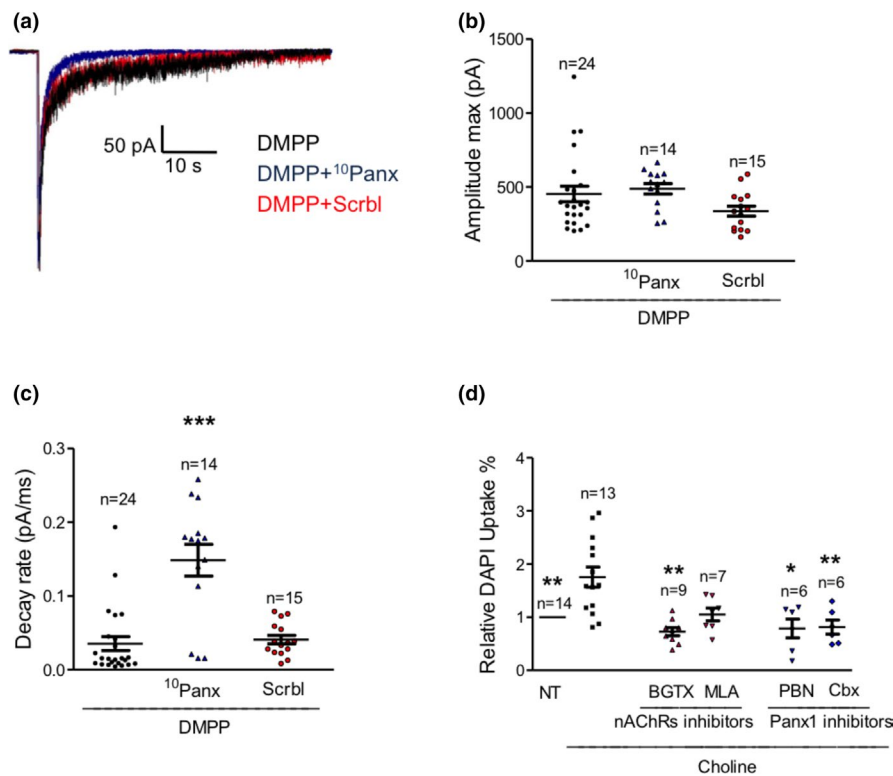


FIGURE 4 Panx1 channel contributions to nicotinic acetylcholine receptor-dependent currents and 4,6-diamidino-2-phenylindole (DAPI) uptake in chromaffin cells. (a–c) Total inward currents induced by a 10 s pulse of 50 μ M dimethylphenylpiperazinium (DMPP) were measured in whole-cell configuration in bovine chromaffin cells. (a) Superimposed representative current traces induced with 50 μ M DMPP (black trace) with or without pretreatment with 200 μ M of ¹⁰Panx1 (blue trace) or the inactive scramble peptide (Scrbl; red trace). (b–c) Each dot represents peak current amplitude or decay rate, respectively, from individual cells. Horizontal lines and whiskers indicate means and SEM. The number of cells recorded from independent cultures ($N \geq 3$) is indicated above each bar. *** $p < .001$ compared to the DMPP condition (Kruskal–Wallis test followed by Dunn's post hoc test). (d) DAPI uptake, induced by 10 mM choline in the absence or presence of 100 nM α -bungarotoxin (BGTX), 10 nM methyllycaconitine, 200 μ M probenecid (PBN) or 5 μ M Cbx, DAPI uptake is represented relative uptake compared to NT condition. Each dot represents average values from individual coverslips. Horizontal lines and whiskers indicate means and SEM, respectively. The number of coverslips analyzed from independent cultures ($N \geq 3$) is indicated above each bar. * $p < .05$, ** $p < .01$ compared with the choline plus PNU condition (one-way ANOVA followed by Bonferroni's post hoc test)

nAChR agonist choline on DAPI uptake, at a concentration (10 mM) previously reported to activate this receptor (Alkondon et al., 1997; Pérez-Alvarez et al., 2012). As shown in Figure 4d, 10 mM choline increased DAPI uptake as compared with the NT condition (1.8 ± 0.2 times over NT uptake). This choline-induced uptake was inhibited with 100 nM BGTX (relative uptake of 0.7 ± 0.1). The relative uptake in the presence of 10 nM MLA was 1.1 ± 0.1 , a value non-significantly different from both NT and choline conditions. Choline-induced DAPI uptake was also inhibited with the Panx1 channel blockers PBN (200 μ M) and Cbx (5 μ M), with resulting relative uptake of 0.8 ± 0.2 and 0.8 ± 0.1 , respectively. Thus, our results point toward the $\alpha 7$ nAChR as an activator of Panx1 channels in bovine chromaffin cells.

Then, we analyzed whether Panx1 channels contribute to the Ca^{2+} signals elicited by activation of $\alpha 7$ nAChRs. Since chromaffin cells express diverse types of nAChRs (for a review see Criado, 2018), the Ca^{2+} signal was induced with 10 mM choline plus 10 μ M PNU-1205696 (as previously described by

Pérez-Alvarez et al., 2012). For these experiments, cytosolic Ca^{2+} signals were measured using epifluorescence time-lapse microscopy in cells loaded with the Ca^{2+} sensitive dye Fura-2. Figure 5a shows averaged fluorescence traces in cells stimulated with choline without or with PNU-1205696 in the absence or presence of Cbx, ¹⁰Panx1 or the scrambled peptide. As shown in Figure 5b, the maximum F/F_0 values in choline-stimulated cells were 1.1 ± 0.02 times over basal levels, but in the presence of PNU-1205696 significantly increased to 1.4 ± 0.02 . Such fluorescence signal was significantly reduced in the presence of 5 μ M Cbx and 200 μ M ¹⁰Panx1 (1.1 ± 0.01 and 1.2 ± 0.02 times over basal levels, respectively). The inactive scrambled peptide caused a partial reduction (1.3 ± 0.2 over basal levels). A modest inhibitory effect of this peptide has also been shown on Panx1 currents in *Xenopus* oocytes (Wang et al., 2007).

Together these results suggest that activation of $\alpha 7$ nAChRs in chromaffin cells opens Panx1 channels, which in turn amplify Ca^{2+} transients.

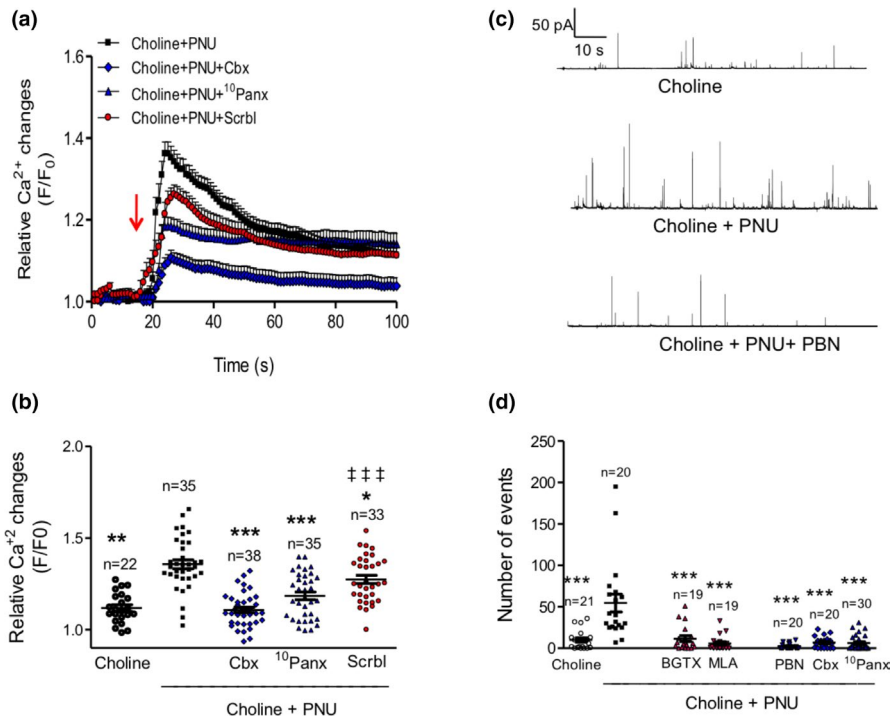


FIGURE 5 Contribution of Panx1 channels to $\alpha 7$ nicotinic acetylcholine receptor dependent Ca^{2+} -signals and exocytosis in chromaffin cells. (a, b) Cytosolic Ca^{2+} signals were measured in Fura-2-loaded chromaffin cells stimulated with 10 mM choline without or with 10 μM PNU-1205696 (PNU), in the absence or presence of 5 μM carbenoxolone (Cbx), or 200 μM of $^{10}\text{Panx1}$ or the scrambled peptide (Scrb1). (a) Cytosolic Ca^{2+} transients are shown as relative changes in fluorescence intensity (F/F_0). (b) Dots represent F/F_0 maximum values from individual cells. Horizontal lines and whiskers indicate means and SEM. The number of cells analyzed from independent cultures ($N \geq 3$) is indicated above each bar. (c, d) Exocytosis was evoked by a 10 s pulse of 10 mM choline without or with pre-treatment with 10 μM PNU in the absence or presence of 100 nM α -bungarotoxin (BGTX), 10 nM methyllycaconitine (MLA), 200 μM probenecid (PBN), 5 μM Cbx, or 200 μM $^{10}\text{Panx1}$, and measured by amperometry. (c) Examples of amperometric traces from chromaffin cells stimulated with choline, choline plus PNU, or choline plus PNU in the presence of PBN. (d) Dots represent the number of amperometric events per cell during the recording. The number of cells analyzed from independent cell cultures ($N \geq 3$) is indicated above each bar. * $p < .05$, ** $p < .01$, *** $p < .001$, compared with the choline plus PNU condition; ††† $p < .001$, compared with the choline condition (one-way ANOVA test followed by Dunnett Multiple comparisons test)

3.5 | Panx1 channel regulates the secretory response elicited by $\alpha 7$ nAChRs in bovine chromaffin cells

Because exocytosis of chromaffin granules is a process triggered by cytosolic Ca^{2+} rises, we analyzed how exocytosis induced by $\alpha 7$ nAChRs is influenced by Panx1 channels. Exocytosis was monitored using carbon fiber amperometry as previously reported (González-Jamett et al., 2017). Figure 5c shows examples of amperometric traces, where each upward spike on the current trace corresponds to the oxidation of the catecholamines released from a single-chromaffin granule (Borges et al., 2008). Figure 5d shows the amount of exocytotic events induced by 10 mM choline without or with 10 μM PNU-1205696 in the absence or presence of 100 nM BGTX, 10 nM MLA, 200 μM PBN or 5 μM Cbx or 200 μM $^{10}\text{Panx1}$. A 10 s pulse with choline induced 10 ± 2 amperometric spikes during the 100 s recording period, whereas the addition of 10 μM PNU-1205696 caused a marked potentiation of the number of amperometric spikes (55 ± 11 spikes in 100 s). The $\alpha 7$ nAChR antagonists BGTX and MLA significantly reduced the amount of amperometric spikes induced

by choline plus PNU-1205696 to 12 ± 3 and 6 ± 2 spikes, confirming the specific activation of $\alpha 7$ nAChRs. The Panx1 channel blockers PBN, Cbx, and $^{10}\text{Panx1}$ also importantly reduced the number of exocytotic events induced by choline plus PNU-1205696, with 2 ± 0.7 , 7 ± 2 , and 6 ± 2 spikes, respectively.

To determine whether Panx1 channels influence the characteristics of individual exocytotic events, we analyzed different amperometric parameters, including the quantal size (Q) that is proportional to the amount of catecholamines released per event, the amplitude of each spike (I_{max}) that indicates the maximum amount of catecholamines reaching the carbon electrode, and the half-width ($t_{1/2}$) that reflects the duration of each release event (Borges et al., 2008). Figure 6a shows a representation of the analyzed parameters. As shown in Figure 6b, PBN significantly reduced Q values, as compared with the choline plus PNU-1205696 condition. However, this parameter was not influenced by Cbx or $^{10}\text{Panx1}$. On the other hand, none of the Panx1 channel blockers significantly affected I_{max} or $t_{1/2}$ (Figure 6c,d).

We also analyzed the characteristics of the current that precedes the amperometric spike, which is referred to as “foot signal.” This

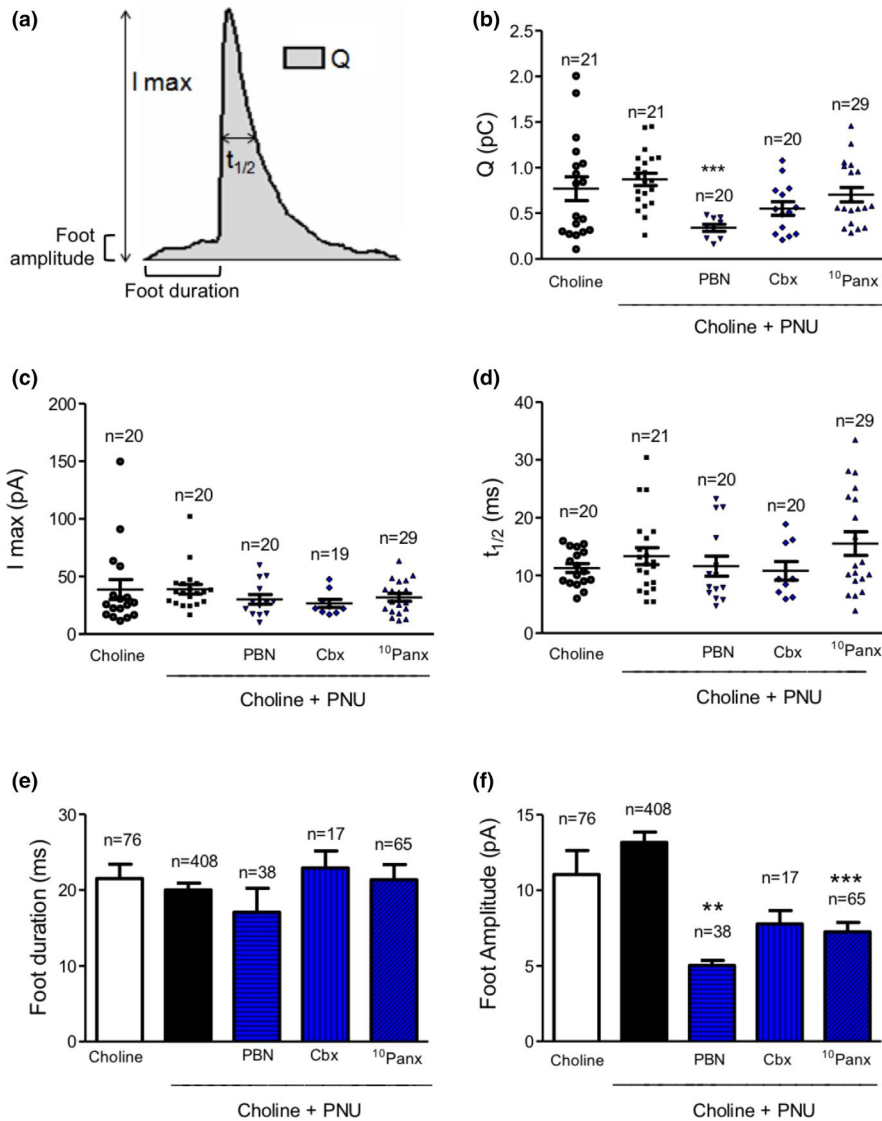


FIGURE 6 Effects of Panx1 channel inhibition on the properties of $\alpha 7$ nicotinic acetylcholine receptor-elicited exocytotic events. (a) Scheme of an amperometric spike with the analyzed parameters: quantal size (Q), amplitude (I_{max}), half width ($t_{1/2}$), and foot duration and amplitude. (b–d) Dots represent averages of median values of Q (b), I_{max} (c), and $t_{1/2}$ (d) from single cells. Horizontal lines and whiskers indicate means and SEM. The number of cells analyzed from independent cultures ($N \geq 3$) is indicated above each. (e, f) Bars represent means \pm SEM of foot duration and amplitude values taken from individual spikes. The number of foot analyzed is indicated above each bar. ** $p < .01$, *** $p < .001$ compared with choline plus PNU-treated cells (Kruskal–Wallis test followed by Dunn's post hoc test)

current reflects the initial release of transmitters through an incipient fusion pore. The duration of the foot signal correlates with the stability of the fusion pore and the amplitude of this signal is proportional to the pore conductance (Albillos et al., 1997; Lindau & de Toledo, 2003). None of the Panx1 channel blockers affected foot duration (Figure 6e), but PBN and 10 Panx significantly reduced foot amplitude (Figure 6f). Thus, Panx1 channels seem to influence the extent of Ca^{2+} -regulated exocytosis, as well as the characteristics of individual exocytotic events.

3.6 | P2X7 purinergic receptors are involved in the Panx1- $\alpha 7$ nAChRs crosstalk

Panx1 channels are apparently not permeable to Ca^{2+} ions (Harcha et al., 2019), instead they reportedly act in concert with the Ca^{2+} permeable P2X7R (Sáez et al., 2017; Tozzi et al., 2018). Therefore, we evaluated whether this receptor contributed to $\alpha 7$ nAChR-elicited Ca^{2+} signals and exocytosis. First, we detected the presence of

P2X7R in SH-SY5Y- $\alpha 7$ and chromaffin cells by immunofluorescence. In SH-SY5Y- $\alpha 7$ cells, P2X7 labeling is observed in both intracellular and cell surface compartments (Figure 7a), whereas this receptor has a more plasma membrane-confined pattern in chromaffin cells (Figure 7b).

We then evaluated whether P2X7R inhibition by the specific inhibitor oxidized ATP (oATP) influenced the Ca^{2+} signal elicited by $\alpha 7$ nAChR activation in both cell types. Therefore, cells were incubated with 100 μ M oATP for 45 min prior to induction of Ca^{2+} signals with 50 μ M DMPP plus PNU-120596 in SH-SY5Y- $\alpha 7$ cells, or 10 mM choline plus 10 μ M PNU-120596 in chromaffin cells. Averaged fluorescence traces in both types of cells are shown in Figure 7c,d and maximum F/F_0 values are indicated in Figure 7e,f. In both cases, inhibition of P2X7R with oATP almost completely abolished the $\alpha 7$ nAChR-elicited cytosolic Ca^{2+} increase. Pre-treatment with the ATP-degrading enzyme apyrase (2 U/ml) also significantly reduced the Ca^{2+} signals in both cell types (Figure 7e,f). These data indicate that stimulation of $\alpha 7$ nAChR types induces ATP release and activation of P2X7R in both cells.

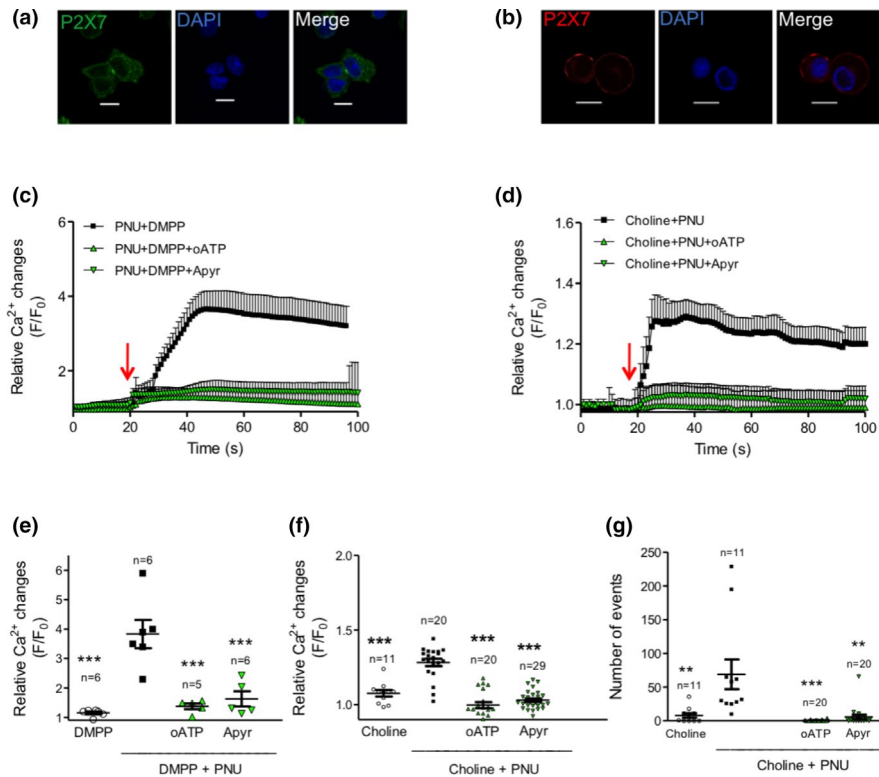


FIGURE 7 $\alpha 7$ nicotinic acetylcholine receptor-induced Ca^{2+} -transients and exocytosis depends on P2X7 receptors. (a, b) Immunofluorescent detection of the P2X7 receptor in SH-SY5Y- $\alpha 7$ and chromaffin cells using an anti-P2X7 antibody, and visualized with an AlexaFluor 488 secondary antibody (a) or AlexaFluor 555 secondary antibody (b). 4,6-diamidino-2-phenylindole staining was used to label the nucleus. Scale bar 10 μm . (c–e) Cytosolic Ca^{2+} signals were measured in Fluo-4 loaded SH-SY5Y- $\alpha 7$ cells stimulated with 50 μM dimethylphenylpiperazinium (DMPP) with or without pre-treatment with the 10 μM PNU-1205696 (PNU) in the presence or absence of 100 μM oxidized ATP (oATP) or 2 U/ml of apyrase. (c) Cytosolic Ca^{2+} transients are shown as relative changes in fluorescence intensity (F/F_0). Data represent mean \pm SEM. (e) Each dot represents averaged F/F_0 maximum values from individual coverslips. At least 10 cells per coverslip were analyzed and fluorescences were averaged. Horizontal lines and whiskers indicate means and SEM, respectively. The number of coverslips analyzed from independent cultures ($N \geq 3$) is indicated above each bar. (d–f) Cytosolic Ca^{2+} signals were measured in Fura-2-loaded chromaffin cells stimulated with 10 mM choline without or with 10 μM PNU, in the absence or presence of 100 μM oATP or 2 U/ml apyrase. (d) Cytosolic Ca^{2+} transients are shown as relative changes in fluorescence intensity (F/F_0). (f) Dots represent F/F_0 maximum values from individual cells. Horizontal lines and whiskers indicate means and SEM. The number of cells analyzed from independent cultures ($N \geq 3$) is indicated above each bar. (g) Exocytosis was evoked by a 10 s pulse of 10 mM choline without or with pre-treatment with 10 μM PNU in the absence or presence of 100 μM oATP or 2 U/ml apyrase. Dots represent the number of amperometric events per cell during the recording. $**p < .01$, $***p < .001$, compared with the choline plus PNU condition (one-way ANOVA followed by Bonferroni's post hoc test)

We also evaluated the effect of oATP and apyrase on DMPP-induced DAPI uptake in order to rule out that this uptake occurs red via P2X7R channels (Sun et al., 2013), or that Panx1 channels are opened after P2X7R activation, which could be activated first by ATP release via exocytosis. As shown in Table S3, oATP and apyrase did not influence DMPP-induced DAPI uptake.

Subsequently, we analyzed how P2X7Rs and ATP release influenced $\alpha 7$ nAChR-elicited exocytosis in chromaffin cells. As shown in Figure 7g, oATP or apyrase drastically reduced the amount of amperometric spikes induced by choline plus PNU-1205696 from 69 ± 22 spikes/100 s to 0.4 ± 0.2 and 2.6 ± 0.8 spikes/100 s, respectively. On the other hand, oATP did not influence the amperometric parameters Q , I_{max} , $t_{1/2}$, foot duration and foot amplitude, whereas apyrase increased $t_{1/2}$ compared with the choline condition, and reduced foot amplitude compared to the PNU-1205696 condition

(Figure S3), suggesting the involvement of additional purinergic receptors.

4 | DISCUSSION

Panx1 channels, $\alpha 7$ nAChRs, and P2X7Rs are co-expressed in adrenal chromaffin cells and SH-SY5Y neuroblastoma cells. Since Panx1 forms non-ligand-gated channels, the signaling mechanisms that induce the opening of this channel are of profound interest. Using different experimental approaches in two cell types, we have found that the opening of Panx1 channels is mediated by $\alpha 7$ nAChR-induced localized Ca^{2+} signals and Src kinase activation, and that Panx1 channels together with P2X7Rs amplify the Ca^{2+} signals and the secretory response in chromaffin cells.



4.1 | $\alpha 7$ nAChR-induced Panx1 channel opening depends on localized Ca^{2+} signals and Src kinases

To study this cross-activation, we took advantage of the SH-SY5Y- $\alpha 7$ cell line that expresses functional $\alpha 7$ nAChRs (Charpantier et al., 2005; Guerra-Álvarez et al., 2015) and Panx1 channels (Alhouayek et al., 2019; Wilkaniec et al., 2017). We found that activation of $\alpha 7$ nAChRs increases Panx1 channel-mediated membrane permeability to DAPI and ATP release. A recent report indicates that Panx1 channel permeability to dyes, such as ethidium, is activated in conditions different to those that promote permeability to anionic molecules (Nielsen et al., 2020). Indeed, Panx1 can form both small- and large-conductance channels that can be activated under different physiological conditions, but whether ATP release occurs via small- or large-conductance channels remains unclear (Chiu et al., 2018). Here we found that DAPI uptake and ATP release exhibit a similar sensibility to Panx1 channel blockers (Figure 2), supporting the idea that DAPI permeability could be a good indicator of Panx1 channel activity in our cell models. ATP release via Panx1 channels has been previously shown in SH-SY5Y cells (Wilkaniec et al., 2017). However, these cells also show Ca^{2+} -dependent exocytosis of dense-cored noradrenergic vesicles (Ou et al., 1998; Zhao et al., 2012). Therefore, we cannot discard that a fraction of ATP could also be released by exocytosis.

Since $\alpha 7$ nAChR are highly permeable to Ca^{2+} (Bertrand et al., 1992, 2015; Delbono et al., 1997; Séguéla et al., 1993), we decided to investigate whether the $\alpha 7$ nAChR-induced Panx1 channel opening depends on cytosolic Ca^{2+} rises. First, we observed that DMPP induced submembrane Ca^{2+} signals in SH-SY5Y- $\alpha 7$ cells, but undetectable global cytosolic Ca^{2+} rises. Only the presence of PNU-120596, an agent that slows $\alpha 7$ nAChR desensitization (Williams et al., 2011) allowed the detection of global cytosolic Ca^{2+} signals. Then the highly localized Ca^{2+} signals induced by $\alpha 7$ nAChR activation might be explained by its fast desensitization (Uteshev, 2012) and/or the efficiency of Ca^{2+} buffering and extrusion systems (Schwaller, 2010), whose inhibition might promote an amplification of the $\alpha 7$ nAChR-elicited Ca^{2+} rise.

In another line of experiments, the absence of external Ca^{2+} or cytosolic Ca^{2+} buffering with BAPTA prevented the $\alpha 7$ nAChR-induced DAPI uptake in SH-SY5Y- $\alpha 7$ cells, suggesting that $\alpha 7$ nAChR-induced Panx1 channel opening depends on highly localized Ca^{2+} signals. The fact that cytosolic Ca^{2+} buffering with EGTA, a Ca^{2+} chelator with a Ca^{2+} on-rate 150 times slower than that for BAPTA (Naraghi & Neher, 1997), did not significantly reduce the $\alpha 7$ nAChR-induced DAPI uptake, further supports the idea that Panx1 channel opening depends on discrete Ca^{2+} microdomains.

Although high cytosolic Ca^{2+} concentrations result in Panx1 channel activation in *Xenopus* oocytes (Locovei et al., 2006), Panx1 currents do not depend on extracellular or cytosolic Ca^{2+} concentrations in HEK293 cells (Ma et al., 2009). These contradictory results may lie in intrinsic intracellular signaling properties of each cellular system. In this respect, Panx1 channels are reportedly activated by Src kinase-mediated phosphorylation (DeLalio et al., 2019; Iglesias

et al., 2008; Lohman et al., 2015). Given that $\alpha 7$ nAChRs can induce Src kinase activation (Dasgupta et al., 2006; Kihara et al., 2001; Li et al., 2019; Shen et al., 2012), we evaluated its involvement. Here, we found that Panx1 channel-mediated DAPI uptake was significantly reduced by Src kinase inhibitors. As Src kinases are known to inactivate $\alpha 7$ nAChRs in a negative feedback loop (Charpantier et al., 2005; Komal et al., 2014), their inhibition would increase $\alpha 7$ nAChR-mediated responses, the effect of PP2 on Panx1-mediated DAPI uptake observed here might be underestimated. Therefore, $\alpha 7$ nAChR-elicited Panx1 channel opening depends on both localized Ca^{2+} signals and Src kinases.

4.2 | Ca^{2+} signals induced by activation of $\alpha 7$ nAChRs are potentiated by P2X7 receptors

In our previous study, we showed the involvement of Panx1 channels in the amplification of Ca^{2+} signals induced by the full nAChR agonist DMPP (Momboisse et al., 2014). Here we observed that Panx1 channels are also responsible for the amplification of $\alpha 7$ nAChR-induced Ca^{2+} signals in both SH-SY5Y- $\alpha 7$ and chromaffin cells. These results reinforce the idea that the nature of the Ca^{2+} signal induced by the activation of nAChRs is not only determined by Ca^{2+} entry through nAChRs and voltage-gated Ca^{2+} channels (Arnaiz-Cot et al., 2008). One possibility is that Panx1 channel opening allows a direct influx of Ca^{2+} through its pore. Indeed, previous reports suggest that Panx1 and Panx3 channels are permeable to Ca^{2+} (Abee et al., 2006; Ishikawa et al., 2011; Yang et al., 2020). However, direct measurement of Ca^{2+} permeability through this channel has not been reported yet. Instead, a study in Panx1 transfected Hela cells shows that opening of Panx1 channels induced ATP release without detectable Ca^{2+} influx (Harcha et al., 2019), suggesting that these channels are not permeable to Ca^{2+} . This is consistent with two independent electrophysiological studies based on determination of the reversal potential properties indicating that Panx1 channels are strictly anion selective (Ma et al., 2012; Romanov et al., 2012). Furthermore, Panx1 channels opened by low oxygen, mechanical stress or elevated extracellular K^+ concentrations, present high unitary conductance and are permeable to ATP (Wang & Dahl, 2018). Therefore, Panx1 channels might contribute to amplification of Ca^{2+} signals through the release of ATP.

As Panx1 channels are known to act together with the P2X7R (Sáez et al., 2017; Tozzi et al., 2018), which conducts Ca^{2+} ions (Egan and Khakh, 2004), we evaluated the contribution of this receptor to $\alpha 7$ nAChR-induced Ca^{2+} signals in SH-SY5Y- $\alpha 7$ cells. We found that inhibition of P2X7Rs by oATP, a widely used P2X7R blocker (Bae et al., 2017; Park et al., 2019; Savio et al., 2018), almost completely abolished $\alpha 7$ nAChR-induced Ca^{2+} signals. This observation is in apparent contrast with the reported functional cross-inhibition between purinergic receptors of the P2X family and nAChRs (Khakh et al., 2000, 2005; Limapichat et al., 2014; Searl et al., 1998). However, most of those studies were performed in heterologous expression systems.

Using the ATP-degrading enzyme apyrase, we further demonstrated that ATP mediates an autocrine loop that regulates the $\alpha 7$ nAChR-induced Ca^{2+} response in SH-SY5Y- $\alpha 7$ cells. As ATP release was inhibited by Panx1 channel blockers, and the Panx1/ATP/P2X7R-mediated amplification of Ca^{2+} signals has been previously described in SH-SY5Y- $\alpha 7$ cells (Wilkaniec et al., 2017), as well as in other cell types (Sáez et al., 2017; Tozzi et al., 2018), we hypothesize that ATP release through Panx1 channels mediates this interaction. However, we cannot rule out that ATP release in this neuronal cell type could also occur through Ca^{2+} -dependent exocytosis (Ou et al., 1998; Zhao et al., 2012).

We also investigated whether the aforementioned feed-back loop was present in chromaffin cells. First, we corroborated that P2X7Rs were expressed in this cell type, as previously identified in rat chromaffin cells (Afework & Burnstock, 1999, 2000; Arribas-Blázquez et al., 2019), and then demonstrated that inhibition of either P2X7Rs with oATP or hydrolysis of extracellular ATP with apyrase decreased $\alpha 7$ nAChR-induced Ca^{2+} signals. Noteworthy, chromaffin cell granules are known to contain, besides catecholamines and peptides, large amounts (~150 mM) of ATP (Winkler & Westhead, 1980). This ATP is co-released during exocytosis (Zhang et al., 2019), enables accumulation of catecholamines inside vesicles (Estévez-Herrera et al., 2016; Klenchin & Martin, 2000), augments the amounts of catecholamine released (Majdi et al., 2019; Larsson et al., 2019), and seems to additionally contribute to the P2X7R-mediated autocrine loop. As Panx1 channel blockers importantly inhibited nAChR-elicited Ca^{2+} signals and exocytosis, these channels might be also involved in this autocrine loop.

4.3 | A functional crosstalk between $\alpha 7$ nAChRs, Panx1 channels, and P2X7 receptor potentiates neurosecretion in chromaffin cells

Since we observed that Panx1 channels, together with P2X7Rs, function as an amplifier mechanism of $\alpha 7$ nAChR-induced Ca^{2+} signals in chromaffin cells, we evaluated their contribution to $\alpha 7$ nAChR-elicited exocytosis. We found that blockage of Panx1 channels greatly reduced the amount of exocytotic events induced by $\alpha 7$ nAChR stimulation, thus confirming the contribution of Panx1 to the secretory response. Since the magnitude of the Ca^{2+} signal might also influence the properties of individual secretory events (Marengo & Cárdenas, 2018), the effects of Panx1 channel blockage on amperometry spike and foot signal properties were also analyzed. We found that the different amperometric parameters were not affected by the Panx1 channel blockers, with the exception of Q that was diminished by PBN, and foot amplitude, which was reduced by PBN and $^{10}\text{Panx1}$. The first parameter reflects the total catecholamine release per event and the latter the catecholamine flux through the initial fusion pore. Both are influenced by cytosolic Ca^{2+} levels (Bretou et al., 2008; Elhamdani et al., 2001; Marom et al., 2010). However, these effects seem to be not related to cytosolic Ca^{2+} levels, as PNU-1205696 did not change these parameters compared

with choline. Cytoskeletal actin also influences these two parameters (González-Jamett et al., 2013, 2017; Olivares et al., 2014), and Panx1 channels are known to interact with this protein network (Boyce et al., 2014). Therefore, this is another possible mechanism that might explain the effects of these Panx1 blockers on Q and foot amplitude.

Both P2X7R inhibition and apyrase treatment almost completely abolished the $\alpha 7$ nAChR-mediated catecholamine secretion. However, only apyrase significantly increased $t_{1/2}$ and reduced foot amplitude, suggesting that other purinergic receptors, in addition to P2X7Rs, are also involved in the regulation of exocytosis in chromaffin cells. Indeed, $G_{i/o}$ -coupled P2Y receptors influence fusion pore expansion in rat chromaffin cells (Chen et al., 2005). Thus, ATP release via Panx1 and/or exocytosis constitutes an autocrine feed-back loop that amplifies exocytosis in chromaffin cells, by mechanism involving P2X7Rs, but additional purinergic receptors may be also involved.

The possible involvement of connexins, which are known to be expressed by the SH-SY5Y cell line (Kim et al., 2016; Sung et al., 2007) and in bovine chromaffin cells (Colomer et al., 2008, 2010; Martin et al., 2003) was not studied in the present work. Therefore, we cannot exclude their participation in this crosstalk. Noteworthy, diverse authors have pointed out that the activation of nAChRs represses expression and function of connexin channels (Cisterna et al., 2020; Colomer et al., 2010; Corsini et al., 2017; Martin et al., 2003).

Taken together, the present findings reveal a new functional interplay between $\alpha 7$ nAChR, Panx1 channels and P2X7Rs that depends on submembrane Ca^{2+} signals, Src kinases, and ATP release, and that might constitute an autocrine loop that amplifies the cytosolic Ca^{2+} signals and secretory response in physiological conditions.

ACKNOWLEDGMENTS

This work has been supported by the FONDECYT (CONICYT, Chile) grants 3180140 (to MCM), 1161672 (to AMC) and 1171240 (to ADM), and P09-022-F from ICM-ANID, Chile. The Centro Interdisciplinario de Neurociencia de Valparaíso (CINV) is a Millennium Institute supported by the Ministerio de Ciencia.

CONFLICT OF INTEREST

The authors declare that there is no conflict of interest regarding the publication of this article.

OPEN RESEARCH BADGES



This article has received a badge for *Open Materials* because it provided all relevant information to reproduce the study in the manuscript. More information about the Open Science badges can be found at <https://cos.io/our-services/open-science-badges/>.

ORCID

Ana M. Cárdenas  <https://orcid.org/0000-0002-8747-4916>



REFERENCES

- Abeele, F. V., Bidaux, G., Gordienko, D., Beck, B., Panchin, Y. V., Baranova, A. V., Ivanov, D. V., Skryma, R., & Prevarskaya, N. (2006). Functional implications of calcium permeability of the channel formed by pannexin 1. *Journal of Cell Biology*, *174*, 535–546. <https://doi.org/10.1083/jcb.200601115>
- Afework, M., & Burnstock, G. (1999). Distribution of P2X receptors in the rat adrenal gland. *Cell and Tissue Research*, *298*, 449–456. <https://doi.org/10.1007/s004410050067>
- Afework, M., & Burnstock, G. (2000). Age-related changes in the localization of P2X (nucleotide) receptors in the rat adrenal gland. *International Journal of Developmental Neuroscience*, *18*, 515–520. [https://doi.org/10.1016/S0736-5748\(00\)00023-X](https://doi.org/10.1016/S0736-5748(00)00023-X)
- Albillos, A., Dernick, G., Horstmann, H., Almers, W., De Toledo, G. A., & Lindau, M. (1997). The exocytotic event in chromaffin cells revealed by patch amperometry. *Nature*, *389*, 509–512. <https://doi.org/10.1038/39081>
- Alhouayek, M., Sorti, R., Gilthorpe, J. D., & Fowler, C. J. (2019). Role of pannexin-1 in the cellular uptake, release and hydrolysis of nandamide by T84 colon cancer cells. *Scientific Reports*, *9*, 7622.
- Alkondon, M., Pereira, E. F., Cartes, W. S., Maelicke, A., & Albuquerque, E. X. (1997). Choline is a selective agonist of $\alpha 7$ nicotinic acetylcholine receptors in the rat brain neurons. *European Journal of Neuroscience*, *9*, 2734–2742. <https://doi.org/10.1111/j.1460-9568.1997.tb01702.x>
- Alvarez, A., Lagos-Cabr e, R., Kong, M., C ardenas, A., Burgos-Bravo, F., Schneider, P., Quest, A. F., & Leyton, L. (2016). Integrin-mediated transactivation of P2X7R via hemichannel-dependent ATP release stimulates astrocyte migration. *Biochimica Et Biophysica Acta*, *1863*, 2175–2188. <https://doi.org/10.1016/j.bbamcr.2016.05.018>
- Ambrosi, C., Gassmann, O., Pranskevich, J. N., Boassa, D., Smock, A., Wang, J., Dahl, G., Steinem, C., & Sosinsky, G. E. (2010). Pannexin1 and Pannexin2 channels show quaternary similarities to connexons and different oligomerization numbers from each other. *Journal of Biological Chemistry*, *285*, 24420–24431. <https://doi.org/10.1074/jbc.M110.115444>
- Antonini, R. A., Benfante, R., Gotti, C., Moretti, M., Kuster, N., Schuderer, J., Clementi, F., & Fornasari, D. (2006). Extremely low-frequency electromagnetic field (ELF-EMF) does not affect the expression of $\alpha 3$, $\alpha 5$ and $\alpha 7$ nicotinic receptor subunit genes in SH-SY5Y neuroblastoma cell line. *Toxicology Letters*, *164*, 268–277. <https://doi.org/10.1016/j.toxlet.2006.01.006>
- Ardiles, A. O., Flores-Mu oz, C., Toro-Ayala, G., C ardenas, A. M., Palacios, A. G., Mu oz, P., Fuenzalida, M., S aez, J. C., & Mart inez, A. D. (2014). Pannexin 1 regulates bidirectional hippocampal synaptic plasticity in adult mice. *Frontiers in Cellular Neuroscience*, *8*, 326. <https://doi.org/10.3389/fncel.2014.00326>
- Arnaiz-Cot, J. J., Gonz alez, J. C., Sobrado, M., Baldelli, P., Carbone, E., Gand a, L., Garc a, A. G., & Hern andez-Guijo, J. M. (2008). Allosteric modulation of alpha 7 nicotinic receptors selectively depolarizes hippocampal interneurons, enhancing spontaneous GABAergic transmission. *Eur. Journal of Neuroscience*, *27*, 1097–1110.
- Arribas-Bl azquez, M., Olivos-Or e, L. A., Barahona, M. V., S anchez de la Muela, M., Solar, V., Jim enez, E., Gualix, J., McIntosh, J. M., Ferrer-Montiel, A., Miras-Portugal, M. T., & Artalejo, A. R. (2019). Overexpression of P2X3 and P2X7 receptors and TRPV1 channels in adrenomedullary chromaffin cells in a rat model of neuropathic pain. *International Journal of Molecular Sciences*, *20*, 155. <https://doi.org/10.3390/ijms20010155>
- Bae, J. Y., Lee, S. W., Shin, Y. H., Lee, J. H., Jahng, J. W., & Park, K. (2017). P2X7 receptor and NLRP3 inflammasome activation in head and neck cancer. *Oncotarget*, *30*, 48972–48982.
- Bao, L., Locovei, S., & Dahl, G. (2004). Pannexin membrane channels are mechanosensitive conduits for ATP. *FEBS Letters*, *572*, 65–68. <https://doi.org/10.1016/j.febslet.2004.07.009>
- Bertrand, D., Bertrand, S., & Ballivet, M. (1992). Pharmacological properties of the homomeric $\alpha 7$ receptor. *Neuroscience Letters*, *146*, 87–90. [https://doi.org/10.1016/0304-3940\(92\)90179-B](https://doi.org/10.1016/0304-3940(92)90179-B)
- Bertrand, D., Lee, C. H. L., Flood, D., Marger, F., & Donnelly-Roberts, D. (2015). Therapeutic potential of $\alpha 7$ nicotinic acetylcholine receptors. *Pharmacological Reviews*, *67*, 1025–1073.
- Borges, R., Camacho, M., & Gillis, K. D. (2008). Measuring secretion in chromaffin cells using electrophysiological and electrochemical methods. *Acta Psychologica*, *192*, 173–184. <https://doi.org/10.1111/j.1748-1716.2007.01814.x>
- Bouzat, C., & Sine, S. M. (2018). Nicotinic acetylcholine receptors at the single-channel level. *British Journal of Pharmacology*, *175*, 1789–1804. <https://doi.org/10.1111/bph.13770>
- Boyce, A. K. J., Wicki-Stordeur, L. E., & Swayne, L. A. (2014). Powerful partnership: Crosstalk between Pannexin 1 and the cytoskeleton. *Frontiers in Physiology*, *5*, 27. <https://doi.org/10.3389/fphys.2014.00027>
- Boyd-Tressler, A., Penuela, S., Laird, D. W., & Dubyak, G. R. (2014). Chemotherapeutic drugs induce ATP release via caspase-gated pannexin-1 channels and a caspase/pannexin-1-independent mechanism. *Journal of Biological Chemistry*, *289*, 27246–27263. <https://doi.org/10.1074/jbc.M114.590240>
- Bravo, D., Ibarra, P., Retamal, J., Pelissier, T., Laurido, C., Hernandez, A., & Constandil, L. (2014). Pannexin 1: A novel participant in neuropathic pain signaling in the rat spinal cord. *Pain*, *155*, 2108–2115. <https://doi.org/10.1016/j.pain.2014.07.024>
- Bretou, M., Anne, C., & Darchen, F. (2008). A fast mode of membrane fusion dependent on tight SNARE zippering. *Journal of Neuroscience*, *28*, 8470–8476. <https://doi.org/10.1523/JNEUROSCI.0860-08.2008>
- Bruzzone, R., Barbe, M. T., Jakob, N. J., & Monyer, H. (2005). Pharmacological properties of homomeric and heteromeric pannexin hemichannels expressed in *Xenopus* oocytes. *Journal of Neurochemistry*, *92*, 1033–1043. <https://doi.org/10.1111/j.1471-4159.2004.02947.x>
- Bruzzone, R., Hormuzdi, S. G., Barbe, M. T., Herb, A., & Monyer, H. (2003). Pannexins, a family of gap junction proteins expressed in brain. *Proceedings of the National Academy of Sciences of the United States of America*, *100*, 13644–13649. <https://doi.org/10.1073/pnas.2233464100>
- Charpentier, E., Wiesner, A., Huh, K. H., Ogier, R., Hoda, J. C., Allaman, G., Raggembass, M., Feuerbach, D., Bertrand, D., & Fuhrer, C. (2005). $\alpha 7$ neuronal nicotinic acetylcholine receptors are negatively regulated by tyrosine phosphorylation and Src-family kinases. *Journal of Neuroscience*, *25*, 9836–9849. <https://doi.org/10.1523/JNEUROSCI.3497-05.2005>
- Chen, X. K., Wang, L. C., Zhou, Y., Cai, Q., Prakriya, M., Duan, K. L., Sheng, Z. H., Lingle, C., & Zhou, Z. (2005). Activation of GPCRs modulates quantal size in chromaffin cells through G(betagamma) and PKC. *Nature Neuroscience*, *8*, 1160–1168.
- Chiu, Y. H., Jin, X., Medina, C. B., Leonhardt, S. A., Kiessling, V., Bennett, B. C., Shu, S., Tamm, L. K., Yeager, M., Ravichandran, K. S., & Bayliss, D. A. (2017). A quantized mechanism for activation of pannexin channels. *Nature Communications*, *8*, 14324. <https://doi.org/10.1038/ncomms14324>
- Chiu, Y. H., Schappe, M. S., Desai, B. N., & Bayliss, D. A. (2018). Revisiting multimodal activation and channel properties of Pannexin 1. *Journal of General Physiology*, *150*, 19–39. <https://doi.org/10.1085/jgp.20171888>
- Cisterna, B. A., Vargas, A. A., Puebla, C., Fern andez, P., Escamilla, R., Lagos, C. F., Matus, M. F., Vilos, C., Cea, L. A., Barnaf e, E., Gaete, H., Escobar, D. F., Cardozo, C. P., & S aez, J. C. (2020). Active acetylcholine receptors prevent the atrophy of skeletal muscles and favor reinnervation. *Nature Communications*, *11*, 1073.
- Colomer, C., Olivos Ore, L. A., Coutry, N., Mathieu, M. N., Arthaud, S., Fontanaud, P., Iankova, I., Macari, F., Thou ennon, E., Yon, L., Anouar,

- Y., & Guérineau, N. C. (2008). Functional remodeling of gap junction-mediated electrical communication between adrenal chromaffin cells in stressed rats. *Journal of Neuroscience*, 26, 6616–6626. <https://doi.org/10.1523/JNEUROSCI.5597-07.2008>
- Colomer, C., Olivos-Oré, L. A., Vincent, A., McIntosh, J. M., Artalejo, A. R., & Guérineau, N. C. (2010). Functional characterization of alpha9-containing cholinergic nicotinic receptors in the rat adrenal medulla: Implication in stress-induced functional plasticity. *Journal of Neuroscience*, 19, 6732–6742.
- Corsini, S., Tortora, M., Rauti, R., & Nistri, A. (2017). Nicotine protects rat hypoglossal motoneurons from excitotoxic death via downregulation of connexin 36. *Cell Death & Disease*, 6, e2881.
- Criado, M. (2018). Acetylcholine nicotinic receptor subtypes in chromaffin cells. *Pflügers Arch*, 470, 13–20. <https://doi.org/10.1007/s00424-017-2050-7>
- Dahl, G. (2015). ATP release through pannexon channels. *Philosophical Transactions of the Royal Society of London. Series B, Biological Sciences*, 370, 1672. <https://doi.org/10.1098/rstb.2014.0191>
- Dasgupta, P., Rastogi, S., Pillai, S., Ordonez-Ercan, D., Morris, M., Haura, E., & Chellappan, S. (2006). Nicotine induces cell proliferation by β -arrestin-mediated activation of Src and Rb–Raf-1 pathways. *The Journal of Clinical Investigation*, 116, 2208–2217.
- Del Barrio, L., Egea, J., León, R., Romero, A., Ruiz, A., Montero, M., Alvarez, J., & López, M. G. (2011). Calcium signalling mediated through $\alpha 7$ and non- $\alpha 7$ nAChR stimulation is differentially regulated in bovine chromaffin cells to induce catecholamine release. *British Journal of Pharmacology*, 162, 94–110. <https://doi.org/10.1111/j.1476-5381.2010.01034.x>
- DeLalio, L. J., Billaud, M., Ruddiman, C. A., Johnstone, S. R., Butcher, J. T., Wolpe, A. G., Jin, X., Keller, T. C. S. 4th, Keller, A. S., Rivière, T., Good, M. E., Best, A. K., Lohman, A. W., Swayne, L. A., Penuela, S., Thompson, R. J., Lampe, P. D., Yeager, M., & Isakson, B. E. (2019). Constitutive SRC-mediated phosphorylation of pannexin 1 at tyrosine 198 occurs at the plasma membrane. *Journal of Biological Chemistry*, 294, 6940–6956. <https://doi.org/10.1074/jbc.RA118.006982>
- Delbono, O., Gopalakrishnan, M., Renganathan, M., Monteggia, L. M., Messi, M. L., & Sullivan, J. P. (1997). Activation of the recombinant human $\alpha 7$ nicotinic acetylcholine receptor significantly raises intracellular free calcium. *Journal of Pharmacology and Experimental Therapeutics*, 280, 428–438.
- Di Virgilio, F., Sarti, A. C., Falzoni, S., De Marchi, E., & Adinolfi, E. (2018). Extracellular ATP and P2 purinergic signalling in the tumour microenvironment. *Nature Reviews Cancer*, 18, 601–618. <https://doi.org/10.1038/s41568-018-0037-0>
- Egan, T. M., & Khakh, B. S. (2004). Contribution of calcium ions to P2X channel responses. *Journal of Neuroscience*, 13, 3413–3420.
- Elhamedani, A., Palfrey, H. C., & Artalejo, C. R. (2001). Quantal size is dependent on stimulation frequency and calcium entry in calf chromaffin cells. *Neuron*, 31, 819–830. [https://doi.org/10.1016/S0896-6273\(01\)00418-4](https://doi.org/10.1016/S0896-6273(01)00418-4)
- Estévez-Herrera, J., Domínguez, N., Pardo, M. R., González-Santana, A., Westhead, E. W., Borges, R., & Machado, J. D. (2016). ATP: The crucial component of secretory vesicles. *Proceedings of the National Academy of Sciences of the United States of America*, 28, E4098–E4106. <https://doi.org/10.1073/pnas.1600690113>
- Garré, J. M., Yang, G., Bukauskas, F. F., & Bennett, M. V. (2016). FGF-1 triggers pannexin-1 hemichannel opening in spinal astrocytes of rodents and promotes inflammatory responses in acute spinal cord slices. *Journal of Neuroscience*, 36, 4785–4801. <https://doi.org/10.1523/JNEUROSCI.4195-15.2016>
- González-Jamett, A. M., Guerra, M. J., Olivares, M. J., Haro-Acuña, V., Baéz-Matus, X., Vásquez-Navarrete, J., Mombosse, F., Martínez-Quiles, N., & Cárdenas, A. M. (2017). The F-actin binding protein cortactin regulates the dynamics of the exocytotic fusion pore through its SH3 domain. *Frontiers in Cellular Neuroscience*, 1, 130. <https://doi.org/10.3389/fncel.2017.00130>
- González-Jamett, A. M., Mombosse, F., Guerra, M. J., Ory, S., Báez-Matus, X., Barraza, N., Calco, V., Houy, S., Couve, E., Neely, A., Martínez, A. D., Gasman, S., & Cárdenas, A. M. (2013). Dynamin-2 regulates fusion pore expansion and quantal release through a mechanism that involves actin dynamics in neuroendocrine chromaffin cells. *PLoS One*, 8, e70638. <https://doi.org/10.1371/journal.pone.0070638>
- Guerra, M. J., González-Jamett, A. M., Báez-Matus, X., Navarro-Quezada, N., Martínez, A. D., Neely, A., & Cárdenas, A. M. (2019). The Ca^{2+} channel subunit Ca v $\beta 2\text{a}$ -subunit down-regulates voltage-activated ion current densities by disrupting actin-dependent traffic in chromaffin cells. *Journal of Neurochemistry*, 151, 703–715.
- Guerra-Álvarez, M., Moreno-Ortega, A. J., Navarro, E., Fernández-Morales, J. C., Egea, J., López, M. G., & Cano-Abad, M. F. (2015). Positive allosteric modulation of alpha-7 nicotinic receptors promotes cell death by inducing Ca^{2+} release from the endoplasmic reticulum. *Journal of Neurochemistry*, 133, 309–319.
- Harcha, P. A., López, X., Sáez, P. J., Fernández, P., Barría, I., Martínez, A. D., & Sáez, J. C. (2019). Pannexin-1 channels are essential for mast cell degranulation triggered during type I hypersensitivity reactions. *Frontiers in Immunology*, 10, 2703. <https://doi.org/10.3389/fimmu.2019.02703>
- Huang, Y. J., Maruyama, Y., Dvoryanchikov, G., Pereira, E., Chaudhari, N., & Roper, S. D. (2007). The role of pannexin 1 hemichannels in ATP release and cell-cell communication in mouse taste buds. *Proceedings of the National Academy of Sciences of the United States of America*, 104, 6436–6441. <https://doi.org/10.1073/pnas.0611280104>
- Hurst, R. S., Hajós, M., Raggenbass, M., Wall, T. M., Higdon, N. R., Lawson, J. A., Rutherford-Root, K. L., Berkenpas, M. B., Hoffmann, W. E., Piotrowski, D. W., Groppi, V. E., Allaman, G., Ogier, R., Bertrand, S., Bertrand, D., & Arneric, S. P. (2005). A novel positive allosteric modulator of the $\alpha 7$ neuronal nicotinic acetylcholine receptor: In vitro and in vivo characterization. *Journal of Neuroscience*, 25, 4396–4405.
- Iglesias, R., Locovei, S., Roque, A., Alberto, A. P., Dahl, G., Spray, D. C., & Scemes, E. (2008). P2X7 receptor-Pannexin1 complex: Pharmacology and signaling. *American Journal of Physiology. Cell Physiology*, 295, C752–C760.
- Ishikawa, M., Iwamoto, T., Nakamura, T., Doyle, A., Fukumoto, S., & Yamada, Y. (2011). Pannexin 3 functions as an ER Ca^{2+} channel, hemichannel, and gap junction to promote osteoblast differentiation. *Journal of Cell Biology*, 193, 1257–1274. <https://doi.org/10.1083/jcb.201101050>
- Jin, Q., Zhang, B., Zheng, X., Li, N., Xu, L., Xie, Y., Song, F., Bhat, E. A., Chen, Y., Gao, N., Guo, J., Zhang, X., & Ye, S. (2020). Cryo-EM structures of human pannexin 1 channel. *Cell Research*, 30, 449–451. <https://doi.org/10.1038/s41422-020-0310-0>
- Khakh, B. S., Fisher, J. A., Nashmi, R., Bowser, D. N., & Lester, H. A. (2005). An angstrom scale interaction between plasma membrane ATP-gated P2X2 and alpha4beta2 nicotinic channels measured with fluorescence resonance energy transfer and total internal reflection fluorescence microscopy. *Journal of Neuroscience*, 29, 6911–6920.
- Khakh, B. S., Zhou, X., Sydes, J., Galligan, J. J., & Lester, H. A. (2000). State-dependent cross-inhibition between transmitter-gated cation channels. *Nature*, 6794, 405–410.
- Kihara, T., Shimohama, S., Sawada, H., Honda, K., Nakamizo, T., Shibasaki, H., Kume, T., & Akaike, A. (2001). $\alpha 7$ nicotinic receptor transduces signals to phosphatidylinositol 3-kinase to block A β -amyloid-induced neurotoxicity. *Journal of Biological Chemistry*, 276, 13541–13546. <https://doi.org/10.1074/jbc.M008035200>
- Kim, I. S., Ganesan, P., & Choi, D. K. (2016). Cx43 mediates resistance against MPP $^{+}$ -induced apoptosis in SH-SY5Y neuroblastoma cells via modulating the mitochondrial apoptosis pathway. *International Journal of Molecular Sciences*, 11, E1819.



- Klenchin, V. A., & Martin, T. F. (2000). Priming in exocytosis: Attaining fusion-competence after vesicle docking. *Biochimie*, 5, 399–407. [https://doi.org/10.1016/S0300-9084\(00\)00208-X](https://doi.org/10.1016/S0300-9084(00)00208-X)
- Komal, P., Gudavicius, G., Nelson, C. J., & Nashmi, R. (2014). T-cell receptor activation decreases excitability of cortical interneurons by inhibiting $\alpha 7$ nicotinic receptors. *Journal of Neuroscience*, 34, 22–35.
- Larsson, A., Majdi, S., Borges, R., & Ewing, A. (2019). Vesicular transmitter content in chromaffin cells can be regulated via extracellular ATP. *ACS Chemical Neuroscience*, 11, 4735–4740. <https://doi.org/10.1021/acscchemneuro.9b00494>
- Li, D. J., Tong, J., Zeng, F. Y., Guo, M., Li, Y. H., Wang, H., & Wang, P. (2019). Nicotinic ACh receptor $\alpha 7$ inhibits PDGF-induced migration of vascular smooth muscle cells by activating mitochondrial deacetylase sirtuin 3. *British Journal of Pharmacology*, 176, 4388–4401.
- Li, S., Tomić, M., & Stojilkovic, S. S. (2011). Characterization of novel Pannexin 1 isoforms from rat pituitary cells and their association with ATP-gated P2X channels. *General and Comparative Endocrinology*, 174, 202–210. <https://doi.org/10.1016/j.ygcen.2011.08.019>
- Limapichat, W., Dougherty, D. A., & Lester, H. A. (2014). Subtype-specific mechanisms for functional interaction between $\alpha 6\beta 4^*$ nicotinic acetylcholine receptors and P2X receptors. *Molecular Pharmacology*, 3, 263–274.
- Lindau, M., & de Toledo, G. A. (2003). The fusion pore. *Biochimica Et Biophysica Acta*, 1641, 167–173. [https://doi.org/10.1016/S0167-4889\(03\)00085-5](https://doi.org/10.1016/S0167-4889(03)00085-5)
- Locovei, S., Bao, L., & Dahl, G. (2006). Pannexin 1 in erythrocytes: Function without a gap. *Proceedings of the National Academy of Sciences of the United States of America*, 103, 7655–7659. <https://doi.org/10.1073/pnas.0601037103>
- Locovei, S., Scemes, E., Qiu, F., Spray, D. C., & Dahl, G. (2007). Pannexin1 is part of the pore forming unit of the P2X(7) receptor death complex. *FEBS Letters*, 581, 483–488.
- Lohman, A. W., Leskov, I. L., Butcher, J. T., Johnstone, S. R., Stokes, T. A., Begandt, D., DeLalio, L. J., Best, A. K., Penuela, S., Leitinger, N., Ravichandran, K. S., Stokes, K. Y., & Isakson, B. E. (2015). Pannexin 1 channels regulate leukocyte migration through the venous endothelium during acute inflammation. *Nature Communications*, 6, 7965.
- Lukas, R. J., Norman, S. A., & Lucero, L. (1993). Characterization of nicotinic acetylcholine receptors expressed by cells of the SH-SY5Y human neuroblastoma clonal line. *Molecular and Cellular Neurosciences*, 4, 1–12. <https://doi.org/10.1006/mcne.1993.1001>
- Ma, W., Compan, V., Zheng, W., Martin, E., North, R. A., Verkhratsky, A., & Surprenant, A. (2012). Pannexin 1 forms an anion-selective channel. *Pflügers Archiv - European Journal of Physiology*, 463, 585–592. <https://doi.org/10.1007/s00424-012-1077-z>
- Ma, W., Hui, H., Pelegrin, P., & Surprenant, A. (2009). Pharmacological characterization of pannexin-1 currents expressed in mammalian cells. *Journal of Pharmacology and Experimental Therapeutics*, 328, 409–418. <https://doi.org/10.1124/jpet.108.146365>
- Majdi, S., Larsson, A., Najafinobar, N., Borges, R., & Ewing, A. G. (2019). Extracellular ATP regulates the vesicular pore opening in chromaffin cells and increases the fraction released during individual exocytosis events. *ACS Chemical Neuroscience*, 5, 2459–2466. <https://doi.org/10.1021/acscchemneuro.8b00722>
- Maldifassi, M. C., Atienza, G., Arnalich, F., López-Collazo, E., Cedillo, J. L., Martín-Sánchez, C., Bordas, A., Renart, J., & Montiel, C. (2014). A new IRAK-M-mediated mechanism implicated in the anti-inflammatory effect of nicotine via $\alpha 7$ nicotinic receptors in human macrophages. *PLoS One*, 9, e108397.
- Marengo, F. D., & Cárdenas, A. M. (2018). How does the stimulus define exocytosis in adrenal chromaffin cells? *Pflügers Archiv - European Journal of Physiology*, 470, 155–167. <https://doi.org/10.1007/s00424-017-2052-5>
- Marom, M., Hagalili, Y., Sebag, A., Tzvier, L., & Atlas, D. (2010). Conformational changes induced in voltage-gated calcium channel Cav1.2 by BayK 8644 or FPL64176 modify the kinetics of secretion independently of Ca^{2+} influx. *Journal of Biological Chemistry*, 285, 6996–7005.
- Martin, A. O., Mathieu, M. N., & Guérineau, N. C. (2003). Evidence for long-lasting cholinergic control of gap junctional communication between adrenal chromaffin cells. *Journal of Neuroscience*, 9, 3669–3678. <https://doi.org/10.1523/JNEUROSCI.23-09-03669.2003>
- Michalski, K., Syrjanen, J. L., Henze, E., Kumpf, J., Furukawa, H., & Kawate Tshimitsu (2020). The Cryo-EM structure of pannexin 1 reveals unique motifs for ion selection and inhibition. *eLife*, 9. <http://dx.doi.org/10.7554/eLife.54670>
- Momboisse, F., Olivares, M. J., Báez-Matus, X., Guerra, M. J., Flores-Muñoz, C., Sáez, J. C., Martínez, A. D., & Cárdenas, A. M. (2014). Pannexin 1 channels: New actors in the regulation of catecholamine release from adrenal chromaffin cells. *Frontiers in Cellular Neuroscience*, 8, 270. <https://doi.org/10.3389/fncel.2014.00270>
- Mou, L., Ke, M., Song, M., Shan, Y., Xiao, Q., Liu, Q., Li, J., Sun, K., Pu, L., Guo, L., Geng, J., Wu, J., & Deng, D. (2020). Structural basis for gating mechanism of Pannexin 1 channel. *Cell Research*, 30, 452–454.
- Murali, S., Zhang, M., & Nurse, C. A. (2014). Angiotensin II mobilizes intracellular calcium and activates pannexin-1 channels in rat carotid body type II cells via AT1 receptors. *Journal of Physiology*, 592, 4747–4762.
- Naraghi, M., & Neher, E. (1997). Linearized buffered Ca^{2+} diffusion in microdomains and its implications for calculation of $[\text{Ca}^{2+}]$ at the mouth of a calcium channel. *Journal of Neuroscience*, 17, 6961–6973.
- Nielsen, B. S., Toft-Bertelsen, T. L., Lolansen, S. D., Anderson, C. L., Nielsen, M. S., Thompson, R. J., & MacAulay, N. (2020). Pannexin 1 activation and inhibition is permeant-selective. *Journal of Physiology*, 2, 361–379. <https://doi.org/10.1113/JP278759>
- Olivares, M. J., González-Jamett, A. M., Guerra, M. J., Baez-Matus, X., Haro-Acuña, V., Martínez-Quiles, N., & Cárdenas, A. M. (2014). Src kinases regulate de novo actin polymerization during exocytosis in neuroendocrine chromaffin cells. *PLoS One*, 9, e99001. <https://doi.org/10.1371/journal.pone.0099001>
- Orellana, J. A., Froger, N., Ezan, P., Jiang, J. X., Bennett, M. V., Naus, C. C., Giaume, C., & Sáez, J. C. (2011). ATP and glutamate released via astroglial connexin 43 hemichannels mediate neuronal death through activation of pannexin 1 hemichannels. *Journal of Neurochemistry*, 118, 826–840.
- Ou, X. M., Partoens, P. M., Wang, J. M., Walker, J. H., Danks, K., Vaughan, P. F., & De Potter, W. P. (1998). The storage of noradrenaline, neuropeptide Y and chromogranins in and stoichiometric release from large dense cored vesicles of the undifferentiated human neuroblastoma cell line SH-SY5Y. *International Journal of Molecular Medicine*, 1, 105–112.
- Park, M., Kim, J., Phuong, N. T. T., Park, J. G., Park, J. H., Kim, Y. C., Baek, M. C., Lim, S. C., & Kang, K. W. (2019). Involvement of the P2X7 receptor in the migration and metastasis of tamoxifen-resistant breast cancer: Effects on small extracellular vesicles production. *Scientific Reports*, 1, 11587.
- Peng, X., Gerzanich, V., Anand, R., Wang, F., & Lindstrom, J. (1997). Chronic nicotine treatment up-regulates $\alpha 3$ and $\alpha 7$ acetylcholine receptor subtypes expressed by the human neuroblastoma cell line SH-SY5Y. *Molecular Pharmacology*, 51, 776–784. <https://doi.org/10.1124/mol.51.5.776>
- Penuela, S., Gehi, R., & Laird, D. W. (2013). The biochemistry and function of pannexin channels. *Biochimica et Biophysica Acta (BBA) - Biomembranes*, 1828, 15–22. <https://doi.org/10.1016/j.bbamem.2012.01.017>
- Pérez-Alvarez, A., Hernández-Vivanco, A., Alonso y Gregorio, S., Tabernero, A., McIntosh, J. M., & Albillos, A. (2012). Pharmacological characterization of native $\alpha 7$ nicotinic ACh receptors and their contribution to depolarization-elicited exocytosis in human chromaffin

- cells. *British Journal of Pharmacology*, 165, 908–921. <https://doi.org/10.1111/j.1476-5381.2011.01596.x>
- Pinheiro, A. R., Paramos-de-Carvalho, D., Certa, M., Costa, C., Magalhães-Cardoso, M. T., Ferreirinha, F., Costa, M. A., & Correia-de-Sá, P. (2013). Bradykinin-induced Ca^{2+} signaling in human subcutaneous fibroblasts involves ATP release via hemichannels leading to P2Y₁₂ receptors activation. *Cell Communication and Signaling*, 11, 70. <https://doi.org/10.1186/1478-811X-11-70>
- Pinheiro, A. R., Paramos-de-Carvalho, D., Certal, M., Costa, M. A., Costa, C., Magalhães-Cardoso, M. T., Ferreirinha, F., Sévigny, J., & Correia-de-Sá, P. (2013). Histamine induces ATP release from human subcutaneous fibroblasts, via pannexin-1 hemichannels, leading to Ca^{2+} mobilization and cell proliferation. *Journal of Biological Chemistry*, 288, 27571–27583.
- Romanov, R. A., Bystrova, M. F., Rogachevskaya, O. A., Sadovnikov, V. B., Shestopalov, V. I., & Kolesnikov, S. S. (2012). The ATP permeability of pannexin 1 channels in a heterologous system and in mammalian taste cells is dispensable. *Journal of Cell Science*, 125, 5514–5523. <https://doi.org/10.1242/jcs.111062>
- Sáez, P. J., Vargas, P., Shoji, K. F., Harcha, P. A., Lennon-Duménil, A. M., & Sáez, J. C. (2017). ATP promotes the fast migration of dendritic cells through the activity of pannexin 1 channels and P2X₇ receptors. *Science Signal*, 506, Eaah7107.
- Sandilos, J. K., Chiu, Y. H., Chekeni, F. B., Armstrong, A. J., Walk, S. F., Ravichandran, K. S., & Bayliss, D. A. (2012). Pannexin 1, an ATP release channel, is activated by caspase cleavage of its pore-associated C-terminal autoinhibitory region. *Journal of Biological Chemistry*, 287, 11303–11311. <https://doi.org/10.1074/jbc.M111.323378>
- Savio, L. E. B., de Andrade, M. P., da Silva, C. G., & Coutinho-Silva, R. (2018). The P2X₇ receptor in inflammatory diseases: angel or demon? *Frontiers in Pharmacology*, 9, 52.
- Schwaller, B. (2010). Cytosolic Ca^{2+} buffers. *Cold Spring Harbor Perspectives in Biology*, 2, a004051. <https://doi.org/10.1101/cshperspect.a004051>
- Searl, T. J., Redman, R. S., & Silinsky, E. M. (1998). Mutual occlusion of P2X ATP receptors and nicotinic receptors on sympathetic neurons of the guinea-pig. *Journal of Physiology*, 510, 783–791. <https://doi.org/10.1111/j.1469-7793.1998.783bj.x>
- Séguéla, P., Wadiche, J., Dineley-Miller, K., Dani, J. A., & Patrick, J. W. (1993). Molecular cloning, functional properties, and distribution of rat brain alpha 7: A nicotinic cation channel highly permeable to calcium. *Journal of Neuroscience*, 13, 596–604. <https://doi.org/10.1523/JNEUROSCI.13-02-00596.1993>
- Shen, J., Xu, L., Sun, S. Y., & Khuri, F. (2012). Deng X (2012) NNK promotes migration and invasion of cancer cells through activation of c-Src, Pkc α and FAK Loop. *Cancer Letters*, 318, 106–113.
- Shigetomi, E., Kracun, S., & Khakh, B. S. (2010). Monitoring astrocyte calcium microdomains with improved membrane targeted GCaMP reporters. *Neuron Glia Biology*, 6, 183–191. <https://doi.org/10.1017/S1740925X10000219>
- Silva, I., Ferreirinha, F., Magalhães-Cardoso, M. T., Silva-Ramos, M., & Correia-de-Sá, P. (2015). Activation of P2Y₆ receptors facilitates nonneuronal adenosine triphosphate and acetylcholine release from urothelium with the lamina propria of men with bladder outlet obstruction. *Journal of Urology*, 194, 1146–1154.
- Silverman, W. R., de Rivero Vaccari, J. P., Locovei, S., Qiu, F., Carlsson, S. K., Scemes, E., Keane, R. W., & Dahl, G. (2009). The pannexin 1 channel activates the inflammasome in neurons and astrocytes. *Journal of Biological Chemistry*, 284, 18143–18151. <https://doi.org/10.1074/jbc.M109.004804>
- Silverman, W., Locovei, S., & Dahl, G. (2008). Probenecid, a gout remedy, inhibits pannexin 1 channels. *American Journal of Physiology. Cell Physiology*, 295, C761–C767. <https://doi.org/10.1152/ajpcell.00227.2008>
- Spray, D. C., & Hanani, M. (2017). Gap junctions, pannexins and pain. *Neuroscience Letters*, 695, 46–52. <https://doi.org/10.1016/j.neulet.2017.06.035>
- Sun, C., Heid, M. E., Keyel, P. A., & Salter, R. D. (2013). The second transmembrane domain of P2X₇ contributes to dilated pore formation. *PLoS One*, 8, e61886. <https://doi.org/10.1371/journal.pone.0061886>
- Sung, J. Y., Lee, H. J., Jeong, E. I., Oh, Y., Park, J., Kang, K. S., & Chung, K. C. (2007). Alpha-synuclein overexpression reduces gap junctional intercellular communication in dopaminergic neuroblastoma cells. *Neuroscience Letters*, 3, 289–293.
- Taly, A., Corringier, P. J., Guedin, D., Lestage, P., & Changeux, J. P. (2009). Nicotinic receptors: Allosteric transitions and therapeutic targets in the nervous system. *Nature Reviews Drug Discovery*, 8, 733. <https://doi.org/10.1038/nrd2927>
- Timóteo, M. A., Carneiro, I., Silva, I., Noronha-Matos, J. B., Ferreirinha, F., Silva-Ramos, M., & Correia-de-Sá, P. (2014). ATP release via pannexin-1 hemichannels mediates bladder overactivity triggered by urothelial P2Y₆ receptors. *Biochemical Pharmacology*, 87, 371–379.
- Tozzi, M., Larsen, A. T., Lange, S. C., Giannuzzo, A., Andersen, M. N., & Novak, I. (2018). The P2X₇ receptor and pannexin-1 are involved in glucose-induced autocrine regulation in β -cells. *Scientific Reports*, 1, 8926. <https://doi.org/10.1038/s41598-018-27281-9>
- Traxler, P., Bold, G., Frei, J., Lang, M., Lydon, N., Mett, H., Buchdunger, E., Meyer, T., Mueller, M., & Furet, P. (1997). Use of a pharmacophore model for the design of EGF-R tyrosine kinase inhibitors: 4-(phenylamino) pyrazolo[3,4-d]pyrimidines. *Journal of Medicinal Chemistry*, 40, 3601–3616.
- Tsuneki, H., Salas, R., & Dani, J. A. (2003). Mouse muscle denervation increases expression of an alpha7 nicotinic receptor with unusual pharmacology. *Journal of Physiology*, 547, 169–179.
- Ugur, M., & Ugur, Ö. (2019). A mechanism-based approach to P2X₇ receptor action. *Molecular Pharmacology*, 95, 442–450. <https://doi.org/10.1124/mol.118.115022>
- Uteshev, V. V. (2012). Somatic integration of single ion channel responses of α 7 nicotinic acetylcholine receptors enhanced by PNU-120596. *PLoS One*, 7, e32951. <https://doi.org/10.1371/journal.pone.0032951>
- Wang, J., & Dahl, G. (2018). Pannexin1: A multifunction and multi-conductance and/or permeability membrane channel. *American Journal of Physiology. Cell Physiology*, 315, C290–C299. <https://doi.org/10.1152/ajpcell.00302.2017>
- Wang, J., Ma, M., Locovei, S., Keane, R. W., & Dahl, G. (2007). Modulation of membrane channel currents by gap junction protein mimetic peptides: Size matters. *American Journal of Physiology-Cell Physiology*, 293, C1112–C1119. <https://doi.org/10.1152/ajpcell.00097.2007>
- Weillinger, N. L., Tang, P. L., & Thompson, R. J. (2012). Anoxia-induced NMDA receptor activation opens pannexin channels via Src family kinases. *Journal of Neuroscience*, 32, 12579–12588. <https://doi.org/10.1523/JNEUROSCI.1267-12.2012>
- Wilkaniec, A., Gąssowska, M., Czapski, G. A., Cieślak, M., Sulkowski, G., & Adamczyk, A. (2017). P2X₇ receptor-pannexin 1 interaction mediates extracellular alpha-synuclein-induced ATP release in neuroblastoma SH-SY5Y cells. *Purinergic Signalling*, 13, 347–361. <https://doi.org/10.1007/s11302-017-9567-2>
- Williams, D. K., Wang, J., & Papke, R. L. (2011). Investigation of the molecular mechanism of the α 7 nicotinic acetylcholine receptor positive allosteric modulator PNU-120596 provides evidence for two distinct desensitized states. *Molecular Pharmacology*, 80, 1013–1032. <https://doi.org/10.1124/mol.111.074302>
- Winkler, H., & Westhead, E. (1980). The molecular organization of adrenal chromaffin granules. *Neuroscience*, 11, 1803–1823.
- Yang, Y., Delalio, L. J., Best, A. K., Macal, E., Milstein, J., Donnelly, I., Miller, A. M., McBride, M., Shu, X., Koval, M., Isakson, B. E., & Johnstone, S. R. (2020). Endothelial Pannexin 1 channels control inflammation by regulating intracellular calcium. *The Journal of Immunology*, 204(11), 2995–3007. <https://doi.org/10.4049/jimmunol.1901089>



- Yeung, A. K., Patil, C. S., & Jackson, M. F. (2020). Pannexin-1 in the CNS: Emerging concepts in health and disease. *Journal of Neurochemistry*, 154(5), 468–485. <https://doi.org/10.1111/jnc.15004>
- Zhang, M., Piskuric, N. A., Vollmer, C., & Nurse, C. A. (2012). P2Y2 receptor activation opens pannexin-1 channels in rat carotid body type II cells: Potential role in amplifying the neurotransmitter ATP. *Journal of Physiology*, 590, 4335–4350. <https://doi.org/10.1113/jphysiol.2012.236265>
- Zhang, Q., Liu, B., Wu, Q., Liu, B., Li, Y., Sun, S., Wang, Y., Wu, X., Chai, Z., Jiang, X., Liu, X., Hu, M., Wang, Y., Yang, Y., Wang, L., Kang, X., Xiong, Y., Zhou, Y., Chen, X., ... Zhou, Z. (2019). Differential co-release of two neurotransmitters from a vesicle fusion pore in mammalian adrenal chromaffin cells. *Neuron*, 102, 173–183. <https://doi.org/10.1016/j.neuron.2019.01.031>
- Zhao, H., Li, L., Fan, H. J., Wang, F., Jiang, L. M., He, P. G., & Fang, Y. Z. (2012). Exocytosis of SH-SY5Y single cell with different shapes cultured on ITO micro-pore electrode. *Molecular and Cellular Biochemistry*, 363, 309–313. <https://doi.org/10.1007/s11010-011-1183-9>
- Zoli, M., Pucci, S., Vilella, A., & Gotti, C. (2018). Neuronal and extraneuronal nicotinic acetylcholine receptors. *Current Neuropharmacology*, 4, 338–349. <https://doi.org/10.2174/1570159X15666170912110450>

SUPPORTING INFORMATION

Additional supporting information may be found online in the Supporting Information section.

How to cite this article: Maldifassi MC, Momboisse F, Guerra MJ, et al. The interplay between $\alpha 7$ nicotinic acetylcholine receptors, pannexin-1 channels and P2X7 receptors elicit exocytosis in chromaffin cells. *J. Neurochem.* 2021;157:1789–1808. <https://doi.org/10.1111/jnc.15186>